

Wigner crystallization in a polarizable medium

G. Rastelli and S. Ciuchi

*Istituto Nazionale di Fisica della Materia and Dipartimento di Fisica
Università dell'Aquila, via Vetoio, I-67010 Coppito-L'Aquila, Italy*

(Dated: February 20, 2019)

We present a variational study of the 2D and 3D Wigner crystal phase of large polarons. The method generalizes that introduced by S. Fratini, P. Quémerais [Mod. Phys. Lett. B **12** 1003 (1998)]. We take into account the Wigner crystal normal modes rather than a single mean frequency in the minimization procedure of the variational free energy. We calculate the renormalized modes of the crystal as well as the charge polarization correlation function and polaron radius. The solid phase boundaries are determined via a Lindemann criterion, suitably generalized to take into account the classical-to-quantum cross-over.

In the weak electron-phonon coupling limit, the Wigner crystal parameters are renormalized by the electron-phonon interaction leading to a stabilization of the solid phase for both low and high polarizability of the medium. Conversely, at intermediate and strong coupling, the behavior of the system depends strongly on the polarizability of the medium.

For weakly polarizable media, a density crossover occurs inside the solid phase when the renormalized plasma frequency approaches the phonon frequency. At low density, we have a renormalized polaron Wigner crystal, while at higher densities the electron-phonon interaction is weakened irrespective of the *bare* electron-phonon coupling.

For strongly polarizable media, the system behaves as a Lorentz lattice of dipoles. The abrupt softening of the internal polaronic frequency predicted by Fratini and Quemerais is observed near the actual melting point only at very strong coupling, leading to a possible liquid polaronic phase for a wider range of parameters.

PACS numbers: 71.30.+h Metal-insulator transitions and other electronic transitions, 71.38.-k Polarons and electron-phonon interactions, 71.45.-d Collective effects

INTRODUCTION

As it was first proposed by Wigner last century [1] the long range Coulomb interaction is able to stabilize a crystal of electrons, which eventually melts upon increasing the density at a quantum critical point. Experiments done on heterostructures [2] and quantum Monte Carlo simulations confirm this scenario [3, 4]. The presence of impurities is known to stabilize the crystal phase in two dimensions [5]. Another mechanism which could help the stabilization of the crystal phase is the effect of a polar material. As a single electron moves in a polar crystal, it polarizes its environment creating a new quasi-particle: a Fröhlich large polaron, with an enlarged effective mass [6, 7]. One expects then an enlargement of the Wigner crystal phase. Interesting properties of the liquid phase in polar doped semiconductors arise also due to the interaction with the polarization, as for example, the mixing between plasmons and longitudinal optical (LO) phonons [8]. Such a mixing can be explained by assuming a long range interaction between the carriers and optical lattice vibrations of the Fröhlich type [9]. The resulting coupled LO-phonon-plasmon modes (CPPMs) are found in polar semiconductors (*n*-type GaP or *p*-type GaAs) [10].

The aim of this work is to study the stabilization of the Wigner Crystal phase and its properties in the presence of a polarizable medium. We consider a general model in which the essential feature is the presence of long range interaction which arise from direct Coulomb

interactions between electrons and from the polarizable medium.

The presence of long range interactions, high polarizability and low carrier density is also a common feature of high-temperature superconductors. Of course, in these materials, short range interactions and lattice effects play an important role. Nonetheless, polarons have been detected by optical measurements in the antiferromagnetic insulating phase of both superconducting and parent cuprates [11, 12, 13]. Moreover, some evidence of strong electron-phonon coupling effects has been given recently in the metallic phase [14]. A new interesting physics is introduced when studying these materials by the fact that the carrier concentration can be varied from very low to sufficiently high density. Prediction on optical properties and more specifically the behavior of the so called Mid Infrared Band (MIR) by varying the doping has been proposed according to polaronic models [15, 16, 28] as well as its interpretation as charge ordering in stripes [17]. A similar behavior has been also found in the optical properties of potassium doped Barium Bismutate [18].

When we consider a system composed of many interacting large polarons we are faced with the problem of screening of *both* electron-electron (e-e) and electron-phonon (e-ph) interactions as we increase the carrier density. A density crossover is therefore expected when the doping concentration is varied so that the plasma frequency approaches the optical longitudinal phonon frequency ω_{LO} .

At high density, phonons cannot follow the much faster plasma oscillations of the electron gas and therefore they do not contribute to the screening of the e-e interactions. On the other hand, the electronic density fluctuations screen the e-ph interaction leading to the undressing of the electrons from their polarization clouds. As a consequence, the polaronic mass renormalization is hugely reduced [19]. In this case, the plasma frequency of the pure electron gas $\omega_P^2 = 4\pi e^2 \rho / m$ is renormalized by the high frequency dielectric constant ε_∞

$$\omega_{P,H}^2 = \frac{\omega_P^2}{\varepsilon_\infty} \quad (\text{high density}) \quad (1)$$

In the high density region, the self energy has been studied by a perturbative approach for weak e-ph coupling ($m_{pol} \simeq m$) in the metallic phase [19]. The validity of this approach is ruled by the condition of $\omega_{LO}^2 \ll \omega_P^2 / \varepsilon_\infty$, since in this regime $\omega_P^2 / \varepsilon_\infty$ is representative of electron density fluctuations. In this case, the electron screening weakens the *effective* e-ph coupling constant and it is argued that the perturbative approach is suitable also for semiconductors which have intermediate values of the *bare* e-ph coupling in the low doping phase. The same results have been obtained at weak and intermediate couplings by a ground state study [20]. An approach which is able to span the strong e-ph coupling regime has been done in ref. [21], where an untrapping transition is found by increasing the density via the plasmon screening of the e-ph interaction. There it is concluded that there is no polaron formation at high density, irrespectively of the strength of the bare e-ph coupling constant.

At low density, the phonon energy scale (phonon-frequency) exceeds the electronic energy scale (plasma frequency). In this limit, the phonons can follow the oscillations of the slower electrons and they screen the e-e interaction. Thus, the frequency of the electron collective modes is renormalized by the static dielectric constant ε_0 . Moreover, in the case of intermediate and strong e-ph coupling, polarons are formed [22] so that the appropriate expression for the general renormalized plasma frequency becomes

$$\omega_{P,L}^2 = \frac{m}{m_{pol}} \frac{\omega_P^2}{\varepsilon_0} \quad (\text{low density}) \quad (2)$$

where m_{pol} is the polaron mass. In the case of *GaAs* the mass renormalization due to the e-ph interaction is negligible, and usually the low density renormalized plasma frequency eq.(2) is used to interpret the experimental data with m , the band mass of the carriers, in place of m_{pol} [10].

In ref.[23] an approximation is developed which allows to study a system of many interacting large polarons in the intermediate/low density regime for weak and intermediate coupling strengths. The phonon degrees of freedom are eliminated by a generalized Lee-Low-Pines

transformation [24] obtaining an effective pair potential between electrons which is non-retarded, with a short range *attractive* term and a long range Coulomb repulsive term, statically screened by ε_0 . The role of the inverse polarizability parameter $\eta = \varepsilon_\infty / \varepsilon_0$ is evident in ref. [23]. In the case of $\eta \ll 1$, which is hereafter reported as the high polarizability regime, repulsive interaction and the retarded phonon-mediated attractive interaction are comparable leading to a softening of the energy of the collective modes at a finite value of the wave vector k , signaling a charge density wave instability. The attractive interaction term between the electrons plays a crucial role also at very low density where the system undergoes a solid/liquid phase transition similar to the Wigner Crystallization (WC) [25]. In ref. [26, 27], a Large Polaron Crystal (LPC) is studied using a path-integral scheme. In ref [27], for $\eta = 1/6$ (high polarizability regime), the authors conclude that in the weak and intermediate e-ph coupling regimes at $T = 0$ the LPC melts toward a polaron liquid, but in the strong coupling regime a phonon instability appears near the melting. The authors argue this behavior from the softening of a long wavelength collective mode due to the e-e dipolar-interaction. A study which shows that the presence of long range order is not necessary for this kind of scenario has been presented in ref. [28] for a simplified model of a classical liquid of interacting dipoles, which are the polarons treated *à la* Feynman. The dipolar mode (internal frequency) is renormalized by the mean field of the other dipoles and it is shown to soften as the density increases, leading to the dissociation of the dipole (polaron).

The present work generalizes the approach of ref. [27] using a formalism which allows to span from high ($\eta \ll 1$) to low polarizability regime ($\eta \simeq 1$). We calculate the boundaries of the solid phase in three as well as in two dimensions and, within the solid phase, the correlation function between the electron density and the charge polarization density. Our results confirm the relevant role of the parameter η in the strong e-ph coupling regime. According to the values of this parameter two distinct behaviours are found:

i) the high polarizability regime in which we found a scenario similar to that of ref. [27] i.e. the melting of the crystal is driven by the instability of the internal polaronic mode. Interestingly our more quantitative prediction push the instability-driven melting toward very strong couplings leaving the possibility of a liquid polaronic phase for a wider range of parameters.

ii) the low polarizability regime, studied here even at strong coupling, in which we found that the screening of the electron-phonon interaction argued in the liquid phase occurs also in the solid phase. Nonetheless e-ph interaction is able to stabilize the crystal against the liquid phase even for moderately polarizable mediums.

This paper is organized as follows: in the first section we illustrate the model and the approximations used, we

introduce the quantities of interest, and we also discuss the Lindemann criterion used to determine the transition temperature. In the second section, we present the results in the three dimensional case. In the third section, the results of the two dimensional case are compared to the those in 3D. The conclusions are reported in the last section. Appendices contain technical details of the calculations.

THE MODEL AND THE METHOD

a) The model

The model describes a system of N interacting electrons in a D -dimensional space, which are coupled to longitudinal (undispersed) optical phonons. The Hamiltonian of the model is a generalization of that introduced by Fröhlich for a single large polaron [29] to N -large polarons [19]. We consider electrons as distinguishable particles. This approximation is justified inside the solid phase, where the overlap between the wavefunctions of different localized electrons is negligible [30]. Using the Path Integral technique [31] phonons can be easily traced out taking advantage of their gaussian nature and we end up with the following partition function [26]:

$$\mathcal{Z} = \oint \prod_i \mathcal{D}[\vec{r}_i(\tau)] e^{-\frac{1}{\hbar} \mathcal{S}_{eff}} \quad (3)$$

where \oint means the functional integration over all cyclic space-time paths of the particles $\vec{r}_i(\tau)$ between zero and $\beta = \hbar/k_B T$. The effective electron action reads

$$\mathcal{S}_{eff} = \mathcal{S}_K + \mathcal{S}_{e-e} + \mathcal{S}_{e-ph-e}^{self} + \mathcal{S}_{e-ph-e}^{dist} + \mathcal{S}_J \quad (4)$$

where

$$\mathcal{S}_K = \int_0^\beta d\tau \sum_i \frac{1}{2} m \left| \dot{\vec{r}}_i(\tau) \right|^2 \quad (5)$$

$$\mathcal{S}_{e-e} = \frac{e^2}{2\varepsilon_\infty} \int_0^\beta d\tau \sum_{i \neq j} \frac{1}{|\vec{r}_i(\tau) - \vec{r}_j(\tau)|} \quad (6)$$

$$\mathcal{S}_{e-ph-e}^{self} = -\frac{\omega_{LO}(1-\eta)e^2}{4\varepsilon_\infty} \int_0^\beta d\tau \int_0^\beta d\sigma \sum_i \frac{D_o(\tau - \sigma)}{|\vec{r}_i(\tau) - \vec{r}_i(\sigma)|} \quad (7)$$

$$\mathcal{S}_{e-ph-e}^{dist} = -\frac{\omega_{LO}(1-\eta)e^2}{4\varepsilon_\infty} \int_0^\beta d\tau \int_0^\beta d\sigma \sum_{i \neq j} \frac{D_o(\tau - \sigma)}{|\vec{r}_i(\tau) - \vec{r}_j(\sigma)|} \quad (8)$$

$$\mathcal{S}_J = \beta \frac{(e\rho_J)^2}{2\varepsilon_0} V \int \frac{d\vec{r}}{r} - \int_0^\beta d\tau \sum_i \int d\vec{r} \frac{e^2 \rho_J / \varepsilon_0}{|\vec{r}_i(\tau) - \vec{r}|} \quad (9)$$

Here e^2 is the electron charge, m is the electron band mass and V is the volume. $(e\rho_J)$ is the static jellium

charge density. The integration of phonons leads to the appearance of retarded e-e interaction terms -eqs.(7,8)-, where the phonon propagator is

$$D_o(\tau) = \frac{\cosh(\omega_{LO}[\beta/2 - \tau])}{\sinh(\beta\omega_{LO}/2)} \quad (10)$$

Using polaronic units (p.u.) ($\hbar\omega_{LO}$ for energy, $1/\omega_{LO}$ for imaginary time τ and $\sqrt{\hbar/m\omega_{LO}}$ for lengths) \mathcal{S}_{e-ph-e} becomes proportional to the dimensionless e-ph coupling constant α defined as

$$\alpha = \frac{e^2}{\sqrt{2}} \frac{1-\eta}{\varepsilon_\infty} \sqrt{\frac{m}{\hbar^3 \omega_{LO}}} \quad (11)$$

while \mathcal{S}_{e-e} will be proportional to the e-e coupling constant

$$\alpha_e = \frac{\sqrt{2}e^2}{\varepsilon_\infty} \sqrt{\frac{m}{\hbar^3 \omega_{LO}}} \quad (12)$$

the ratio $\alpha_e/\alpha = 2/(1-\eta)$ is thus solely determined by η : when $\eta \simeq 1$ the Coulomb repulsion overwhelms the attraction mediated by phonons, while they become comparable for $\eta \ll 1$. Therefore, in the Fröhlich model, the inverse polarizability parameter $\eta = \varepsilon_\infty/\varepsilon_0$ rules the relative weight between the repulsive and attractive (phonon-mediated) interactions. This attraction can lead to a bi-polaronic ground state at high polarizability ($\eta \leq \eta_c$) and strong coupling ($\alpha > \alpha_c(\eta_c)$). The value η_c has been determined by a low-density variational theory as $\eta_c = 0.08$ [32].

We have investigated the system for two values of η , representative respectively of the high and low polarizability regimes, and several values of the e-ph coupling α . We choose respectively $\eta = 1/6$ as in ref.[27], which gives $\alpha_e/\alpha = 2.4$, and $\eta = 0.90519$ so that the coupling α_e/α is increased by a factor of ten. For these values of η , no bi-polaron ground state exists.

As a last point we want to stress that the pure electron gas limit of action eq. (4) can be reached when $\alpha = 0$ and α_e is finite, which implies $\eta = 1$. On the other hand, for a given η , $\alpha_e \rightarrow 0$ as $\alpha \rightarrow 0$. It should be noted, however, that the limit of zero e-ph interaction is somehow unphysical in the presence of a given inverse polarizability parameter of the system: as can be seen by the calculation of appendix B, when $\varepsilon_0 \neq \varepsilon_\infty$, the interaction with the polarizable medium is *necessary* to stabilize the crystal phase.

b) The harmonic variational approximation in the solid phase

We generalize the harmonic variational approach originally introduced in ref.[26] to study the model eq.(4). First of all we recall here the variational theory in the path integral formalism. Let us consider a suitable trial

action \mathcal{S}_T which depends on some variational parameters. Substituting \mathcal{S}_{eff} with \mathcal{S}_T in eq.(3) we obtain the partition function \mathcal{Z}_T for the trial action and the free energy associated to it $\mathcal{F}_T = -k_B T \ln \mathcal{Z}_T$. Then the exact free energy can be expressed as

$$\mathcal{F} = \mathcal{F}_T - k_B T \ln \left\langle e^{-\frac{1}{\hbar} \Delta \mathcal{S}} \right\rangle_T \quad (13)$$

where $\Delta \mathcal{S} = \mathcal{S}_{eff} - \mathcal{S}_T$ and the mean value $\langle \dots \rangle_T$ is

$$\langle \dots \rangle_T = \frac{1}{\mathcal{Z}_T} \oint \prod_i \mathcal{D}[\vec{r}_i(\tau)] (\dots) e^{-\frac{1}{\hbar} \mathcal{S}_T} \quad (14)$$

The variational free energy is obtained by a cumulant expansion of the logarithm appearing in eq. (13). At first order in $\Delta \mathcal{S}$ it reads:

$$\mathcal{F}_V = \mathcal{F}_T + \frac{1}{\beta} \langle \Delta \mathcal{S} \rangle_T \quad (15)$$

where $\mathcal{F}_V \geq \mathcal{F}$.

A generic average of an electronic observable on the effective action is given by

$$\langle \dots \rangle_{eff} = \frac{1}{\mathcal{Z}} \oint \prod_i \mathcal{D}[\vec{r}_i(\tau)] \dots [\{\vec{r}_i\}] e^{-\frac{1}{\hbar} \mathcal{S}_{eff}} \quad (16)$$

and its cumulant expansion reads

$$\langle \dots \rangle_{eff} = \langle \dots \rangle_T + \left\langle \dots \frac{\Delta \mathcal{S}}{\hbar} \right\rangle_T + \langle \dots \rangle_T \left\langle \frac{\Delta \mathcal{S}}{\hbar} \right\rangle_T + \theta(\Delta \mathcal{S}^2) \quad (17)$$

To define a suitable trial action we proceed in two steps as in ref.[26]. First we treat the self interaction term $\mathcal{S}_{e-ph-e}^{self}$ of eq. (7) *a la Feynman* [33, 34]. Therefore we substitute $\mathcal{S}_{e-ph-e}^{self}$ with \mathcal{S}_{Feyn}

$$\mathcal{S}_{Feyn} = \frac{(v^2 - w^2)mw}{8} \sum_i \int_0^\beta d\tau \int_0^\beta d\sigma D_V(\tau - \sigma) |\vec{r}_i(\tau) - \vec{r}_i(\sigma)|^2 \quad (18)$$

v and w are the two variational parameters. The variational propagator $D_V(\tau)$ is given by eq. (10) with w replacing ω_{LO} .

As a second step, we treat the \mathcal{S}_{e-e} , \mathcal{S}_J eqs.(6,9) and the distinct part ($\mathcal{S}_{e-ph-e}^{dist}$) eq.(8) of \mathcal{S}_{eff} in eq.(4) by means of a harmonic approximation. Expressing the position of the electrons around the Wigner lattice points as $\vec{r}_i = \vec{u}_i + \vec{X}_i$ where \vec{X}_i are the vectors of the Bravais lattice (b.c.c. in 3D, hexagonal in 2D) and omitting the constant terms of the solid phase potential energy, we obtain the following harmonic variational action:

$$\mathcal{S}_T = \mathcal{S}_K + \mathcal{S}_{Feyn} + \mathcal{S}_J^H + \mathcal{S}_{e-e}^H + \mathcal{S}_{e-ph-e}^{H,dist} \quad (19)$$

where

$$\mathcal{S}_K = \int_0^\beta d\tau \sum_i \frac{1}{2} m |\dot{\vec{u}}_i(\tau)|^2 \quad (20)$$

$$\begin{aligned} \mathcal{S}_{e-J}^H + \mathcal{S}_{e-e}^H &= \int_0^\beta d\tau \sum_i \frac{1}{2} m \frac{\omega_W^2}{\varepsilon_0} |\vec{u}_i(\tau)|^2 \\ &+ \int_0^\beta d\tau \frac{e^2}{2\varepsilon_\infty} \sum_{i \neq j} \vec{u}_j(\tau) \overline{\vec{u}}_i(\tau) \end{aligned} \quad (21)$$

$$\mathcal{S}_{e-ph-e}^{H,dist} = -\frac{\omega_{LO} e^2}{4\varepsilon} \sum_{i \neq j} \int_0^\beta d\tau \int_0^\beta d\sigma D_o(\tau - \sigma) \vec{u}_j(\sigma) \overline{\vec{u}}_i(\tau) \quad (22)$$

In eq.(21), the Wigner frequency is defined as usual in 3D as $\omega_{W,3D}^2 = \omega_P^2/3$ (for the 2D case see eq.(108) in Appendix B). The force constants $[\overline{\mathcal{I}_{ij}}]_{\alpha\beta}$ are obtained through a harmonic expansion for the Coulomb potential (see appendix B). In our calculations, we neglect the anharmonic terms in $\Delta \mathcal{S}$ of eq. (15), therefore we get

$$\mathcal{F}_V = \mathcal{F}_T + \frac{1}{\beta} \left\langle \mathcal{S}_{e-ph-e}^{self} - \mathcal{S}_{Feyn} \right\rangle_T \quad (23)$$

We have minimized \mathcal{F}_V/N varying w, v at given density and temperature keeping α and η fixed. Minimization is constrained by a convergence condition on the gaussian integrals appearing in \mathcal{F}_V . The constrained minimization procedure is described in appendix C.

So far, the discussed scheme appears very similar to the one of ref.[26]. However, we stress that the \mathcal{F}_V , which we have minimized to obtain the variational parameter v and w , contains the hetero-interaction terms \mathcal{S}_{e-e}^H and $\mathcal{S}_{e-ph-e}^{H,dist}$, which are not included in the minimization procedure of ref. [26]. Moreover, we have also used the *full* action \mathcal{S}_T eq.(19) to calculate the mean electronic fluctuation $\langle u^2 \rangle$ which we have used in the Lindemann rule, as explained in the following section.

c) Lindemann rule and phase diagrams

To determine the solid-liquid transition we use the phenomenological Lindemann criterion, suitably generalized to take into account the classical-to-quantum cross-over [35]:

$$\frac{\langle |\vec{u}|^2 \rangle}{d_{n.n.}^2} = \gamma^2 (\eta_q) \quad (24)$$

in the l.h.s. of eq. (24) we have the Lindemann ratio between the mean fluctuation of the electrons around its equilibrium position and the nearest neighbors distance $d_{n.n.}$. When it exceeds a critical value (r.h.s. of eq. (24)), the solid melts.

The mean thermal fluctuation is calculated to zero order in the variational cumulant expansion eq. (17) of the trial action eq.(19), and $d_{n.n.}$ is given by the lattice structure (see also Appendix D).

Contrary to the classical liquid-solid transition, where the Lindemann rule predicts the full melting line using a constant $\gamma = \gamma_{cl}$, in the case of a quantum crystal an interpolating formula for γ is necessary to determine the melting line as obtained by comparing the free-energies of the two phase calculated in the quantum simulations [3]. Hence the analytic expansion of the quantum corrections to the classical free energy respect to the quantum parameter η_q and the zero-temperature melting density provides the interpolating function (r.h.s. of eq.24) for $\gamma(\eta_q)$ [35]. η_q is defined for the pure electron gas as the ratio between zero point and thermal activation energies as:

$$\eta_q = \frac{\hbar\omega_p}{2k_B T}. \quad (25)$$

We have chosen for the function $\gamma(\eta_q)$ the form of refs. [36, 37]:

$$\gamma(T, r_s) = \gamma_q - \frac{\gamma_q - \gamma_{cl}}{1 + A\eta_q^2} \quad (26)$$

Formula (26) has a single interpolation parameter A which we take as $A = 1.62 \cdot 10^{-2}$ in 3D [36] and $A = 3 \cdot 10^{-2}$ in 2D [37].

The chosen value of $\gamma_{cl} = 0.155$ is such that the classical transition lines ($T = 2/\Gamma_c r_s$ a.u.) are recovered in both the 3D ($\Gamma_c = 172$ from ref. [36]) and 2D ($\Gamma_c = 135$ from ref. [37]) cases. The value $\gamma_q = 0.28$ is chosen to reproduce the zero temperature quantum transition in 3D ($r_s = 100$ a.u. from ref. [36]) and 2D ($r_s = 37$ a.u. from ref. [37]).

Roughly speaking, the transition curve is limited by the classical line $T = (2/\Gamma_c) 1/r_s$ and the quantum melting $1/r_s = 1/r^c$. The actual transition curve is a smooth interpolation between these two limiting behaviors. Of course, the precise knowledge of the interpolation formula (i.e. the knowledge of parameters appearing in it) is critical only for the determination of the transition line at high temperatures (see fig.1).

We notice that the particular values of the parameters entering in eq.(26) depend on the kind of statistics (boson, fermion) and on the system parameters only via the ratio η_q . This parameter depends on the mass of the particles via ω_p , which measures the zero point energy of the oscillator which eventually melts [38]. Therefore, to generalize the Lindemann criterion to the interacting large polaron system we are left with the alternative of choosing between the electron and the polaron effective mass in eqs. (25,26).

The polaron exists as a well defined quasiparticle when both $k_B T \ll \hbar\omega_{LO}$ [39] and $\hbar\bar{\omega}_P \ll \hbar\omega_{LO}$. The second

condition relies on the effectiveness of the e-ph interaction, as explained in the introduction. Therefore, if both conditions are fulfilled, we have to replace ω_P in eq. (25) by $\bar{\omega}_P$ given by eq. (2). In this case, between the classical ($\eta_q \simeq 0$) and quantum melting ($\eta_q \rightarrow \infty$), we have a polaronic Wigner Crystal. This is the case of the high polarizability ($\eta = 0.17$).

For low polarizability ($\eta = 0.9$), a cross-over occurs inside the solid phase when $\hbar\bar{\omega}_P \sim \hbar\omega_{LO}$ and the coupling is intermediate or strong, as it will be discussed in details later on. In this case, we still have a classical melting of polaronic quasi-particles, but the quantum melting involves the undressed electrons. In the classical regime (low density), the transition line does not depend appreciably on the quantum parameter, as γ attains its classical limit ($\eta_q \rightarrow 0$). In the quantum regime at high density and low temperatures ($\eta_q \rightarrow \infty$) the function γ eq. (26) saturates to its quantum value γ_q and the density r_c of the quantum melting does not depend of the choice for the quantum parameter η_q . Instead, a pronounced dependency on the actual value of the quantum parameter is expected in the calculation of the melting line at high temperatures and intermediate densities.

For $\eta = 0.9$ we choose the high density estimate $\omega_P/\sqrt{\epsilon_\infty}$ as the plasma frequency entering in eq. (25). This choice produces, in the intermediate temperature/density region, an upward deviation (fig. 1 lower panel) from the classical slope. This is a drawback of our approximation, which is however correct at low temperatures for both low and high density.

We finally discuss to which extent we use the Lindemann criterion in 2D, and more generally on the applicability of the harmonic theory in 2D. This is related to the well known problem of the existence of two dimensional crystalline long-range order at finite temperature [40]. In a pure electron gas, for $T = 0$, this problem does not arise and the properties of the system in the harmonic approximation have been studied extensively [41, 42]. The general statement for the classical impossibility of 2D crystalline long-range order was first pointed out by Peierls [43]. Landau [44] gave a general argument according to which fluctuations destroy crystalline order possessing only a one or two dimensional periodicity. The first microscopic treatment of the problem (not valid in case of Coulomb interaction) is due to Mermin [40]: his proof is based on Bogolyubov's inequality that leads to the conclusions that the Fourier component of the mean density is zero for every vector k in the thermodynamic limit. Motivated by the interest of the 2D electron gas, Mermin's proof was critically re-examined for the long range potential [45, 46]. We discuss here the argument of Peierls for the 2D electron crystal. The mean square thermal fluctuations of a generic classical particle diverges in two dimensions for an infinite harmonic crystal. At low density, we have $\eta_q \simeq 0$ and the mean electronic fluctuation can be approximated by the

classical value

$$\langle u^2 \rangle_{Cl,WC} = \frac{Dk_B T}{2m\omega_P^2} \mathcal{M}_{-2} \quad (27)$$

$$\mathcal{M}_{-2} = \int d\omega \rho(\omega) \frac{\omega_P^2}{\omega^2} \quad (28)$$

where \mathcal{M}_{-2} is the dimensionless second inverse moment of the density of the states (DOS) of charge fluctuation normal modes in the pure WC ($\rho(\omega)$). Since long-wavelength acoustical vibrational modes scale as $\omega = c_s k$, the DOS is given at low energies by $\rho(\omega) \sim \omega$ for $\omega \rightarrow 0$ [47] and the integral eq.(27) diverges logarithmically. However, a lower cut-off in the frequency spectrum, which exists for a large but finite system normally studied in the laboratory [47] or in a computer simulation [4, 48], removes the logarithmic divergence. We have chosen a cut-off frequency which corresponds to a fixed number of particles $N \simeq 5 \cdot 10^5$. The dependence of the cut-off is discussed in appendix A. There and later on it is shown that our results are cut-off independent for low temperatures and density near the quantum critical point. Therefore we will discuss 2D case only in this region.

e) Correlation functions and polaron radius

We now introduce the correlation functions between the electron and the polarization densities for a system with N electrons, and a measure of the polaron radius.

The polarization density vector of the medium is associated to the optical phonon modes $Q_{\vec{k}}$ through the relation [7]:

$$\vec{P}(\vec{r}) = \sum_{\vec{k}} i \frac{\omega_{LO}}{\sqrt{4\pi\epsilon V}} \frac{\vec{k}}{|\vec{k}|} e^{i\vec{k}\vec{r}} Q_{\vec{k}}. \quad (29)$$

The induced charge density is defined by [7]

$$n_{ind.}(\vec{r}) = -\frac{1}{e} \vec{\nabla} \cdot \vec{P}(\vec{r}) \quad (30)$$

Correlation between a given electron and the induced charge density can be defined as:

$$C_1(\vec{r}', \vec{r}) = \frac{\langle \rho_1(\vec{r}) n_i(\vec{r}') \rangle}{\langle \rho_1(\vec{r}) \rangle} \quad (31)$$

with $\rho_1(\vec{r}) = \delta(\vec{r} - \vec{r}_1)$. In eq.(31) we have chosen the appropriate normalization for the correlation function between *one* electron and the polarization. Integrating out the phonons we arrive at the following expression, in which we express all quantities in terms of averages weighted by the effective action eqs.(4,16)

$$C_1(\vec{r}', \vec{r}) = \frac{1}{\bar{\epsilon}} \int_0^\beta d\tau \frac{\omega_{LO}}{2} D_o(\tau) \frac{\langle \rho_1(\vec{r}) \rho(\vec{r}', \tau) \rangle_{eff}}{\langle \rho_1(\vec{r}) \rangle_{eff}} \quad (32)$$

In eq.(32) $\rho(\vec{r}', \tau)$ is the path density defined by:

$$\rho(\vec{r}', \tau) = \delta(\vec{r}' - \vec{r}_1(\tau)) + \sum_{i \neq 1} \delta(\vec{r}' - \vec{r}_i(\tau)) \quad (33)$$

where we have explicitly separated the contribution $\rho_1(\vec{r}', \tau)$ due to the electron 1 from the remainder. The first contribution in r.h.s. of eq. (33) give rise to a self term in the correlation function eq. (32) given by

$$C_1^{self} = \frac{1}{\bar{\epsilon}} \int_0^\beta d\tau \frac{\omega_{LO}}{2} D_o(\tau) \frac{\langle \rho_1(\vec{r}) \rho_1(\vec{r}', \tau) \rangle_{eff}}{\langle \rho_1(\vec{r}) \rangle_{eff}} \quad (34)$$

Notice that in the limit of a single isolated polaron, this correlation function reduces to the one evaluated in ref. [39]. Assuming an electron at origin ($\vec{r} = 0$), we have C_1^{self} depending only on \vec{r}' . The radial induced charge density $g(r)$ can be defined as

$$g(r) = r^{D-1} \int d^D \Omega C_1^{self}(\vec{r}) \quad (35)$$

Using this function, we can define, as a measure of the polaronic radius, the square root of the second moment of $g(r)$

$$R_p = \left(\int_0^\infty dr r^2 g(r) \right)^{1/2} \quad (36)$$

The actual calculation is carried on to the zero order eq. (14) in the variational cumulant expansion eq. (17). From eqs. (34,35) as well as from the results reported in appendix E we have

$$R_p = \left(D \frac{\omega_{LO}}{2} \int_0^\beta d\tau D_o(\tau) \ell^2(\tau) \right)^{1/2} \quad (37)$$

where the characteristic length $\ell^2(\tau)$ is defined by

$$d(\tau) = \frac{\langle |\vec{u}(\tau) - \vec{u}|^2 \rangle_T}{D} \quad (38)$$

$$\ell^2(\tau) = d(\tau) \left[1 - \frac{d(\tau)}{4 \langle |\vec{u}(0)|^2 \rangle_T / D} \right] \quad (39)$$

RESULTS IN 3D

Here we compare the low ($\eta = 0.9$) and high ($\eta = 1/6$) polarizability cases in 3D. For each polarizability, the electron-phonon coupling constant α spans from weak to strong coupling regime: $\alpha = 1, 3, 5, 7, 9, 11, 13, 15$.

Phase diagrams obtained through the Lindemann criterion are shown in figs. 1 and 2 where the solid-liquid transition lines of the LPC are compared to that of the pure Wigner crystal. A common feature of both the

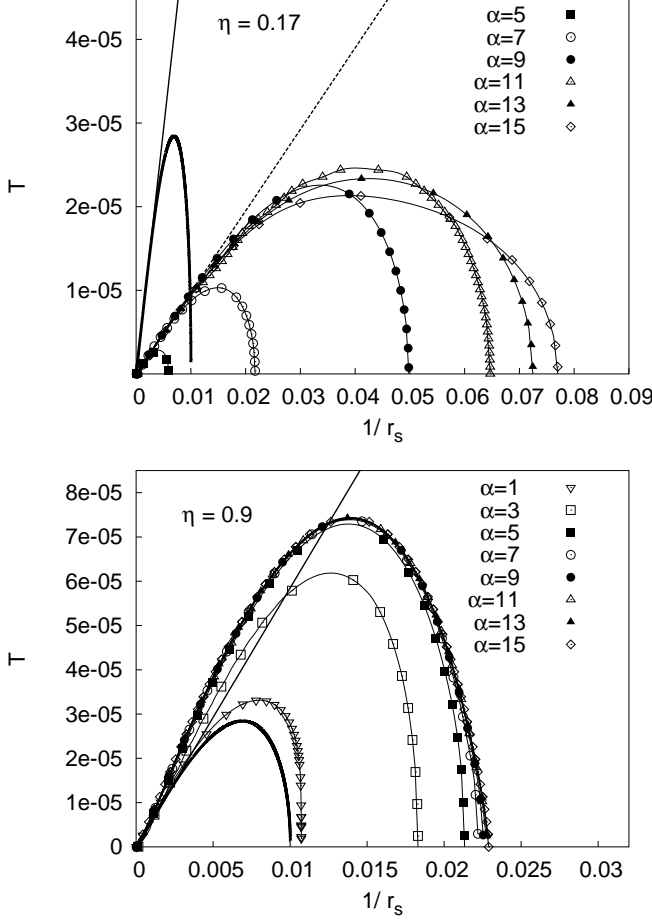


FIG. 1: Phase diagrams for a 3D LPC for $\eta = 0.17$ (upper panel) and $\eta = 0.9$ (lower panel). Atomic units (a.u.) are used for temperature and r_s . We chose for effective band mass $m = m_e$ and $\varepsilon_\infty = 1$. Solid phase is enclosed below transition lines. In both the upper and the lower panels continuous bold curve is the pure WC transition line and solid line gives the classical melting. In the upper panel dashed line is the renormalized classical melting.

low and high polarizability cases is the enlargement of the solid phase as far as e-ph coupling increases (fig.2). However, in both cases, the solid phase cannot be stabilized for any density by increasing the e-ph interaction, and the quantum melting point saturates at a maximum value when the e-ph coupling is very strong. The reason of this behavior is different in the low and high polarizability cases, and will be discussed below. As we have noticed at the end of sect. I a) the pure WC melting is not recovered as $\alpha \rightarrow 0$, since we work at fixed value of η , as is evident in the $\eta = 0.17$ case. We now focus on the weak e-ph coupling region, where stabilization of the solid phase by e-ph interaction is effective (renormalized melting region).

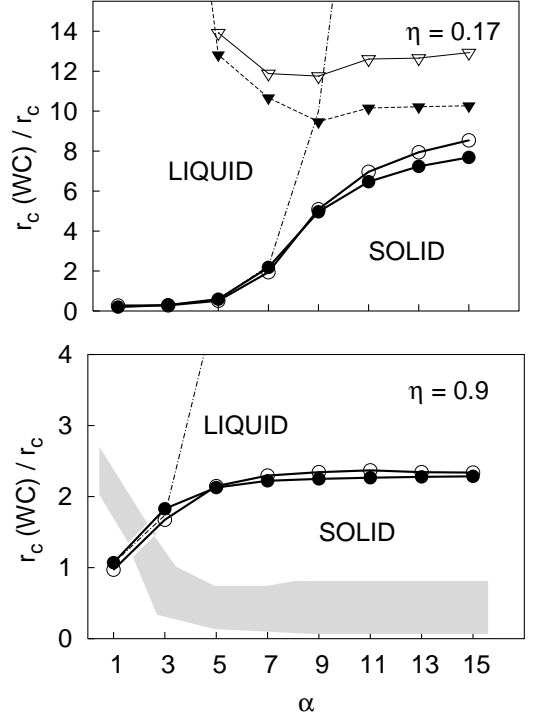


FIG. 2: Zero temperature phase diagram in the 2D (open symbols) and 3D (solid symbols) cases. In 2D α has been scaled according the zero density limit. Circles are the scaled quantum melting r_c vs e-ph coupling constant α . Dashed line is the renormalized quantum melting transition curve from eq.(46). Upper panel: $\eta = 0.17$. Triangles locates the softening of ω_{pol} (see fig.9). Lower panel: $\eta = 0.9$. The shaded area encloses the cross-over region inside the solid phase.

a) Weak e-ph coupling

At weak e-ph coupling, in both the high and low polarizability cases, melting occurs at a density such that $\omega_{P,L} \ll \omega_{TO}$, i.e. in a region where phonons are much faster than density fluctuations.

According to the discussion made in the introduction, the effect of the e-ph interaction is a renormalization the electron mass $m \rightarrow m_{pol}$ and a screening of the electron-electron interaction $e^2 \rightarrow e^2/\varepsilon_0$. At a given density, the eigenfrequencies of the LPC density fluctuations are renormalized by the same factor ($\omega_P \rightarrow \omega_P/\varepsilon_0 m_{pol}$) of eq. (2). m_{pol} can be deduced by variational parameters reminding that in the Feynman variational scheme S_{Feyn} eq.(18) can be obtained by integrating out a set of fictitious particles (R_i) of mass $M_T = m[(v^2/w^2) - 1]$ which interact elastically ($K_T = m(v^2 - w^2)$) with each electron. The polaron mass is $m_{pol} = m + M_T$ and is given by:

$$m_{pol} = m \frac{v^2}{w^2}. \quad (40)$$

The internal frequency and the reduced mass of the two particle system are

$$v^2 = \frac{KT}{\mu} \quad \text{with} \quad \frac{1}{\mu} = \frac{1}{m} + \frac{1}{M_T}. \quad (41)$$

Let us first consider the classical transition. In this case, by the previous consideration, we can estimate the ratio between electronic fluctuations in LPC and in WC by using eq. (27) which gives

$$\frac{\langle u^2 \rangle_{CL,LPC}}{\langle u^2 \rangle_{CL,WC}} = \frac{1}{\varepsilon_0} \quad (42)$$

then by Lindemann criterion eq. (24) and by eq. (27) at a given density, the critical temperature ratio also equals $1/\varepsilon_0$. Therefore, the slope of the classical transition line is lowered by the same ε_0 factor, as can be seen in fig. 1 (upper panel), where ε_0 is appreciably large.

The quantum melting is ruled by the zero point fluctuations of the electronic oscillations. A zero temperature estimate for the pure WC gives

$$\langle u^2 \rangle_{WC} = \frac{\hbar D}{2m\omega_P} \mathcal{M}_{-1} \quad (43)$$

$$\mathcal{M}_{-1} = \int d\omega \rho(\omega) \frac{\omega_P}{\omega} \quad (44)$$

where \mathcal{M}_{-1} is the dimensionless inverse moment of the WC DOS. If we scale the mass and the plasma frequency according to eq. (2), taking into account eq.(43), we get for the LPC

$$\frac{\langle u^2 \rangle_{Q,LPC}}{\langle u^2 \rangle_{Q,WC}} = \left(\frac{m\varepsilon_0}{m_{pol}} \right)^{1/2} \left(\frac{r_s}{r_s(WC)} \right)^{3/2}. \quad (45)$$

then using Lindemann criterion we obtain at the quantum critical point ($r_s = r_c$)

$$\frac{r_c(WC)}{r_c} = \frac{m_{pol}}{m\varepsilon_0}. \quad (46)$$

eq.(46) generalizes the result of the ref.[26] where the Lindemann rule was discussed within a mean field approach.

Eq.(46) quantitatively describes quantum melting in the low polarizability case only at small coupling ($\alpha \leq 3$). When α exceeds this value, in the low polarizability case, a cross-over between a polaronic and a non polaronic phase is found inside the solid phase and the estimate of eq. (46) no longer describes quantum melting. A complete discussion of the case is deferred to section II c).

At high polarizability, quantum melting is given by eq. (46) up to intermediate values of $\alpha \simeq 7$. Notice that at weak coupling the mass renormalization is weak, but phonon screening through ε_0 dominates, leading to quantum melting at lower densities than in a purely electronic Wigner Crystal (upper panel fig.1). On the other

hand, upon increasing the coupling, the mass renormalization leads to an increase of the critical density because of the mass renormalization entering the zero point fluctuations. Since m_{pol} scales as $\sim \alpha^4$ in strong coupling, eq.(46) predicts a divergence of the quantum melting density. As shown in figs. 1 (upper panel) and in fig.2 (upper panel), the quantum melting density saturates to an α -independent value at strong coupling, and the prediction of eq. (46) is no longer valid.

We will see in the next subsection that deviation from the prediction of eq. (46) arise from different reasons in low and high polarizability cases.

b) A simplified model

To explain the behavior of the LPC in the intermediate/strong e-ph coupling regime, it is useful to map the trial action to a simplified model, as introduced in ref. [27]. Assuming the variational parameter $w = \omega_{LO}$, the action of the harmonic variational action \mathcal{S}_T eq.(19) is obtained by a non-retarded Lagrangian where the electrons interact with each other and with all the fictitious particles. After integration of the fictitious particles, the effective electronic lagrangian generated by the simplified model corresponds exactly to the lagrangian of the action \mathcal{S}_T eq.(19) with the parameter $w = \omega_{LO}$.

This approximation restricts the space of variational parameters, and therefore gives rise to a worse estimate for the free energy. Nonetheless, it allows to describe the physics of the system in a simplified fashion.

Each WC's branch is splitted in two branches for the LPC and the frequencies of the system are [27]

$$\Omega_{\pm}^2 = \frac{1}{2} \left[\frac{\omega_{s,\vec{k}}^2}{\varepsilon_{\infty}} + \omega_{pol}^2 \pm \sqrt{\left(\frac{\omega_{s,\vec{k}}^2}{\varepsilon_{\infty}} + \omega_{pol}^2 \right)^2 - 4\omega_{LO}^2 \frac{\omega_{s,\vec{k}}^2}{\varepsilon_0}} \right] \quad (47)$$

$$\omega_{pol}^2 = v^2 - \frac{1-\eta}{\varepsilon_{\infty}} \omega_W^2 \quad (48)$$

where $\omega_{s,\vec{k}}$ are the WC frequencies characterized by wave vector \vec{k} and by the branch index s . The polaronic frequency ω_{pol} eq.(48) is defined as the $k = 0$ mode of the polaronic branches (optical modes) of eq.(47) [27] and it represents the internal frequency of oscillation of the electron inside its polarization well.

The expression for the fluctuation $\langle u^2 \rangle_{eq}$ of electrons around their equilibrium value in the simplified model is easily obtained by inserting $w = \omega_{LO}$ in the zero order term of the variational cumulant expansion $\langle u^2 \rangle_T$ (Appendix D) associated to the harmonic variational approximation action \mathcal{S}_T eq.(19).

The \pm branches in eq.(47) give rise to a natural split-

ting of contributions to the fluctuation (fig.3)

$$\frac{\langle u^2 \rangle_{eq}}{d_{n.n.}^2} = \frac{\langle u^2 \rangle_+}{d_{n.n.}^2} + \frac{\langle u^2 \rangle_-}{d_{n.n.}^2} \quad (49)$$

$$\langle u^2 \rangle_+ = \int d\omega \rho(\omega) \frac{\Omega_+^2 - \omega_{LO}^2}{\Omega_+^2 - \Omega_-^2} \frac{\hbar D}{2m\Omega_+} \coth\left(\frac{\hbar\Omega_+}{2k_B T}\right) \quad (50)$$

$$\langle u^2 \rangle_- = \int d\omega \rho(\omega) \frac{\Omega_-^2 - \omega_{LO}^2}{\Omega_-^2 - \Omega_+^2} \frac{\hbar D}{2m\Omega_-} \coth\left(\frac{\hbar\Omega_-}{2k_B T}\right) \quad (51)$$

where Ω_{\pm} are the solutions of eq. (47) keeping ω fixed. Notice that if we take a single Wigner frequency being representative of the electronic spectrum ($\rho(\omega) = \delta(\omega - \omega_W)$) we recover the results of ref. [26].

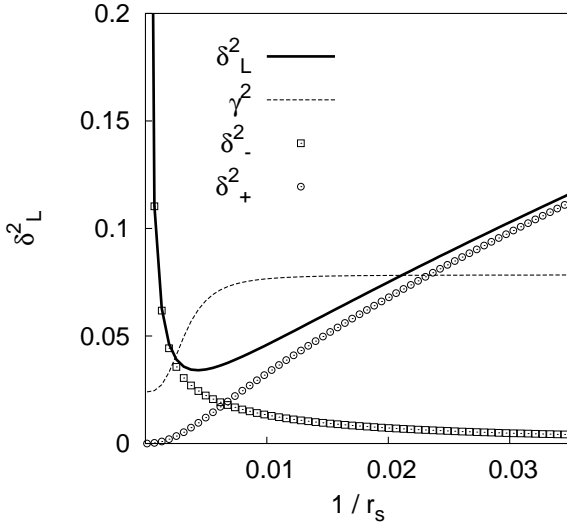


FIG. 3: The Lindemann ratio (solid line) $\delta_L^2 = \langle u^2 \rangle / d_{n.n.}^2$ and the function γ (dashed line) eq.(24) for $\eta = 0.9$ and $\alpha = 5$ $T = 1.8 \cdot 10^{-5}$ (a.u.). Contributions $\delta_{\pm}^2 = \langle u^2 \rangle_{\pm} / d_{n.n.}^2$ eqs.(49,50,51) are also shown.

At low density $\langle u^2 \rangle_+$ and $\langle u^2 \rangle_-$ are respectively associated to internal and the center of mass motion of the oscillating electron-polarization system. To see this explicitly let us notice that at low density the parameter

$$\epsilon_{s,\vec{k}} = \omega_{s,\vec{k}}^2 / (\epsilon_0 v^2) \quad (52)$$

is small for all (\vec{k}, s) . Expanding eqs.(47) for all frequencies of normal modes (k, s) and using eq.(40) we get the solutions [27] :

$$\Omega_-^2 \simeq \frac{m}{m_{pol}} \frac{\omega_{s,\vec{k}}^2}{\epsilon_0} \quad (53)$$

$$\Omega_+^2 \simeq \omega_{pol}^2 + \frac{\omega_{s,\vec{k}}^2}{\epsilon_{\infty}} \quad (54)$$

In the low density regime the frequencies spectrum is decomposed into the WC frequencies with effective mass m_{pol} and dielectric constant ϵ_0 (Ω_-) which represents the low frequencies associated to the oscillation of the center of mass of the system composed by electron and its fictitious particle (see lower panel fig.4) and the polaronic optical frequencies (Ω_+) weakly dispersed around the frequency ω_{pol} (see upper panel fig.4).

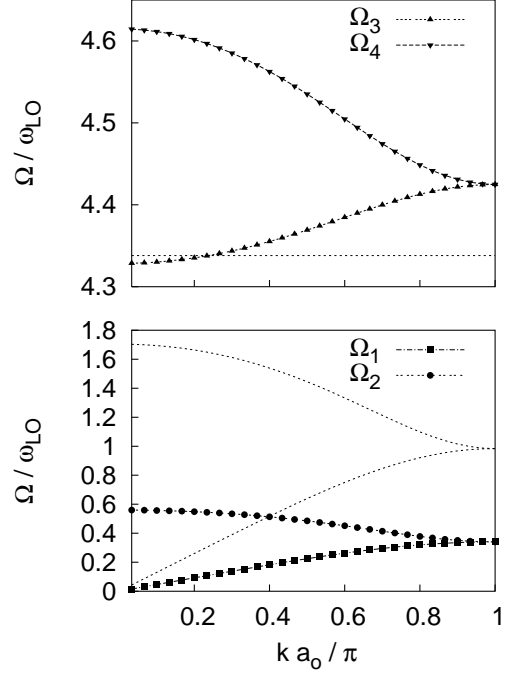


FIG. 4: Eigenfrequencies of the simplified model as a function of \vec{k} along the direction (100) for $\alpha = 5$ and $\eta = 0.9$. The inverse $1/r_s = 2.55 \cdot 10^{-3}$ (a.u.) at the same temperature of fig. 3. Density is close to the classical liquid-solid transition. Lower panel: Ω_1 and Ω_2 (renormalized WC frequencies) eq.(53). For comparison are shown the WC frequencies (dashed line). Upper panel: Ω_3 and Ω_4 polaronic optical frequencies eq.(54). Dashed line is the parameter v .

Writing the electron position \vec{u} in terms of the center of mass \vec{R}_b

$$\vec{R}_b = \frac{m\vec{u} + M_T \vec{R}_T}{m + M_T}. \quad (55)$$

and of internal distance of the system

$$\vec{\rho} = \vec{u} - \vec{R}_T. \quad (56)$$

we have the following expressions

$$\vec{u} = \vec{R}_b + \frac{M_T}{m + M_T} \vec{\rho} \quad (57)$$

In the low density regime, expanding the electron fluctuation eq.(49) with respect to the parameter $\epsilon_{s,\vec{k}}$ eq.(52) for all frequencies, it is possible to associate each term of the fluctuation in eqs.(51,50) to a definite degree of freedom, i.e. a fluctuation of the center of mass

$$\langle u^2 \rangle_- \simeq \int d\omega \rho(\omega) \frac{\hbar D \coth\left(\hbar \sqrt{\frac{m}{m_{pol}} \frac{\omega^2}{\epsilon_0}} / 2k_B T\right)}{2m_{pol} \sqrt{\frac{m}{m_{pol}} \frac{\omega^2}{\epsilon_0}}} \quad (58)$$

and a fluctuation associated to the internal dipolar mode

$$\langle u^2 \rangle_+ \simeq \left(\frac{M_T}{m + M_T} \right)^2 \frac{\hbar D}{2\mu\omega_{pol}} \coth\left(\frac{\hbar\omega_{pol}}{2k_B T} \right) \quad (59)$$

c) Low polarizability: cross-over in solid phase

In this regime ($\eta \sim 1$), the repulsive interactions among electrons overwhelm the attractive interactions due to the polarizability of the background, as can be seen by the relative weight of e-e and e-ph interaction coupling constant eqs.(11,12). However, self-trapping effects are still present at least at strong coupling and at low density, where electrons are localized.

At low density within the crystal, the polarization follows adiabatically the electron. The solid phase is a Wigner crystal made of polarons with an effective mass determined by the e-ph interaction. As far as the density increases (inside the solid phase), the electronic kinetic energy increases due to the progressive localization of the particles. The polarization cannot follow the electronic motion anymore and the polarons disappear as quasi particles. This condition *does not imply the dissolution of the crystal*, which can still be stable if the charge fluctuations around Wigner lattice points are sufficiently small.

To estimate the density dependence of the frequencies eq.(47), let us substitute $\omega_{s,\vec{k}}$ by the plasma frequency ω_P . Results are reported in fig.5, which illustrates the density cross-over. In the low density limit ($r_s \rightarrow \infty$) $\Omega_- = \omega_{P,L}$ eq.(2) while Ω_+ converges to $\omega_{pol} \simeq v$ the internal frequency eq.(48). In this case, the electrons are far apart, and the “external” harmonic field generated by the surrounding electrons of the crystalline array is weak ($K_e \sim e^2/r_s^3$). Therefore the frequency of electron oscillation ($\omega_P^2 \sim K_e/m$) can be lower than that of the phonon (ω_{LO}), and the polarization follows the electron oscillation. The polaron vibrates as a whole with a lower frequency $K_e/m_{pol} \sim \omega_P^2 (m/m_{pol}\epsilon_0)$. The polarization charge distribution is undisturbed as a first approximation, so that the internal polaronic frequency of the electron inside its polarization well doesn’t change.

By increasing the density, we approach the opposite limit of strong external field. Now the frequency associated to this field is too large and the polarization cannot follow the electron oscillation, so that each electron becomes undressed from its polarization cloud. In

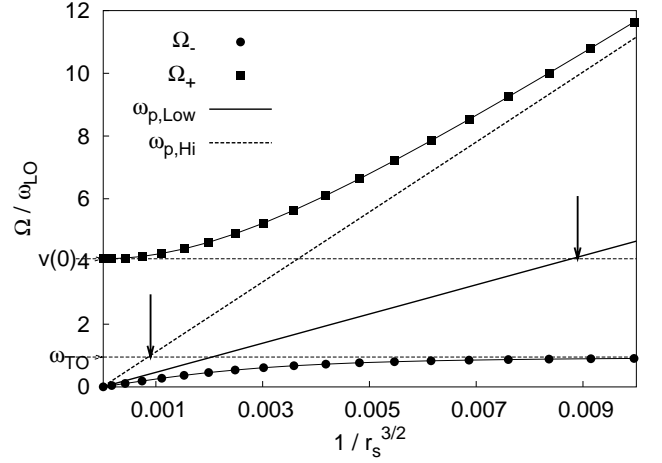


FIG. 5: Filled points are the typical frequencies of the simplified model obtained from eq.(47) with $\omega_{s,k} = \omega_P$ for $\alpha = 5$ and $\eta = 0.9$. Solid line is the low density renormalized plasma frequency eq.(2). Dashed line the high density renormalized plasma frequency eq.(1). Arrows mark the crossover region (see text).

this case Ω_+ eq.(47) approaches $\omega_P/\sqrt{\epsilon_\infty}$, the high density renormalized plasma frequency eq.(1), while $\Omega_- \simeq \sqrt{\epsilon_\infty/\epsilon_0}\omega_{LO} = \omega_{TO}$ is the characteristic renormalized frequency of the polarization.

We notice that at low density Ω_- eq.(2) gives a measure of the frequency of carrier density fluctuations, while in the opposite limit of high density, the same role is played by Ω_+ eq.(1).

As we can see from fig.5, the cross-over amplitude is determined by the conditions $\omega_{P,H} \simeq \omega_{TO}$ and $\omega_{P,L} \simeq v$.

Inside the cross-over region, the electrons and the polarization modes are mixed as in the liquid phase CPPM [9] but the role played there by the phonon frequency ω_{LO} is here played by the internal polaronic frequency.

The cross-over of the renormalization of the plasma frequency from low to high density regime doesn’t imply the melting of the crystal. Indeed, it is observed within the boundary of the solid phase estimated by Lindemann criterion. This behavior is even more clear once we consider the electronic fluctuations which enter in the Lindemann criterion. Taking into account the dispersion of the frequencies, the two term eqs.(50,51) of the Lindemann ratio of the simplified model are compared to the Lindemann ratio from variational calculation in fig.3. From the data shown in fig.3 it can be seen that the leading term for the Lindemann ratio at the classical melting is $\delta_-^2 = \langle |u|^2 \rangle_- / d_{n.n.}^2$, which is associated to the fluctuation of the center of mass eq.(58). Of course, in the classical region quantum fluctuations are ineffective, the electrons and its polarization cloud behave as a single classical par-

ticle with mass m_{pol} . The term $\delta_+^2 = \langle |u|^2 \rangle_+ / d_{n.n.}^2$ associated to the internal polaronic frequencies eq.(59) is indeed negligible.

Upon further increasing the density we enter in the high density region where we meet eventually the Lindemann criterion for quantum melting. To analyze this region we notice that the condition $\epsilon_{s,\vec{k}} \gg 1$ can be fulfilled by the majority of normal modes at high density, eq.(52). Of course, long wavelength acoustical and even “optical” modes in 2D have vanishing energies, but their spectral weight is low enough to be neglected in the following considerations.

Expanding eq.(47) in $1/\epsilon_{s,\vec{k}}$ we get

$$\Omega_- \simeq \sqrt{\frac{\epsilon_\infty}{\epsilon_0}} \omega_{LO} \quad (60)$$

$$\Omega_+ \simeq \frac{\omega_{s,\vec{k}}}{\sqrt{\epsilon_\infty}} \quad (61)$$

In fig. 6 the general solutions of eq.(47) are shown for all the branches of the simplified model near the quantum melting.

The branches (Ω_2, Ω_4) which results as splitting of optical model of the Wigner crystal $\omega_{s,\vec{k}}^{opt}$ are well described by approximation of eqs.(60,61).

The frequency dispersion (Ω_1, Ω_3) of the modes which originate from the splitting of acoustical branches of the Wigner crystal is also reported. While at short wavelength, the dispersion approaches the estimates given in eqs.(60,61) the long wavelength part of the spectrum is conversely described by eqs.(53,54).

Thus we have that at the quantum melting the low energy part of the spectrum still behaves as in the low density regime. The modes depicted in the lower part of fig.6 belongs to this part of the spectrum.

A measure of the wave-vector below which we have this behavior can be obtained by the condition $\epsilon_{s,\vec{k}} = 1$. The associated energy scale is given by $\omega_c^2 = m\omega_{LO}^2 / (\epsilon_0 m_{pol})$. Contrary to low density regime eqs.(58,59), it is not possible to associate to each term of the fluctuation eqs.(50,51) a definite degree of freedom. However, expanding the electron fluctuation with respect to the parameter $\epsilon_{s,\vec{k}}$ for the frequencies $\omega_{s,k} < \omega_c$ and with respect to the parameter $1/\epsilon_{s,\vec{k}}$ for the frequencies $\omega_{s,k} > \omega_c$, using eq. (49) the electron position fluctuations can be approximated by:

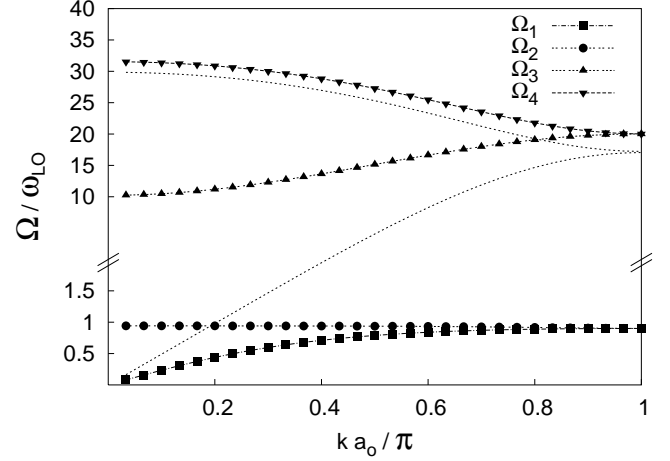


FIG. 6: Frequencies of the system in the simplified model as a function of \vec{k} along the direction (100), for $\alpha = 5$ and $\eta = 0.9$. $1/r_s = 2.10^{-2}$ (a.u.) at the same temperature of fig. 3. Density is close to the quantum melting. $\Omega_1\Omega_3$ results from the splitting of the WC branch (eq.(47)). $\Omega_2\Omega_4$ results from the splitting of the high frequency WC optical branch (eqs.(60,61)). For comparison are shown the pure WC frequencies (dotted lines).

$$\langle u^2 \rangle_- \simeq \int_0^{\omega_c} d\omega \rho(\omega) \frac{\hbar D \coth\left(\hbar \sqrt{\frac{m}{m_{pol}\epsilon_0}} \omega / 2k_B T\right)}{2m_{pol} \sqrt{\frac{m}{m_{pol}\epsilon_0}} \omega} \quad (62)$$

$$\begin{aligned} \langle u^2 \rangle_+ &\simeq \left(\frac{M_T}{m + M_T}\right)^2 \frac{\hbar D}{2\mu\omega_{pol}} \coth\left(\frac{\hbar\omega_{pol}}{2k_B T}\right) \int_0^{\omega_c} d\omega \rho(\omega) \\ &+ \int_{\omega_c}^{\infty} d\omega \rho(\omega) \frac{\hbar D}{2m \frac{\omega}{\sqrt{\epsilon_\infty}}} \coth\left(\hbar \frac{\omega}{\sqrt{\epsilon_\infty}} / 2k_B T\right) \end{aligned} \quad (63)$$

Notice that the interpretation of the fluctuations associated to electronic motion in this case is different from that valid at low density. In particular the high energy contribution (the second term of eq. (63) represents a Wigner crystal-like fluctuation with a low energy cut-off. This is the largest contribution to the fluctuation at quantum melting (fig. 3) and does not depend on e-ph interaction.

As shown in fig. 3, the leading term of fluctuations at quantum melting is $\langle u^2 \rangle_+$. This is due to the vanishing of the spectral weight associated to the low frequencies $\omega < \omega_c$ at high density (eq.(62)).

The saturation of the quantum melting point can be seen in the phase diagram of fig. 1 (lower panel). Two comments are needed. First, in the case of very low e-ph coupling, the density crossover does not occur inside the solid phase. Therefore, these arguments do not apply. The quantum melting point depends on the e-ph coupling as we have discussed in the previous section. However a

saturation of the quantum melting density is observed clearly in fig.1 for intermediate and strong coupling. As a second point we have to emphasize that the quantum melting density *is not* that of a purely electronic Wigner crystal.

This fact can be explained by writing the total electron fluctuation as the sum of the two terms $\langle u^2 \rangle_{Hi}$ and $\langle u^2 \rangle_{Low}$ where $\langle u^2 \rangle_{Hi}$ is the contribution to fluctuations of modes having energies higher (lower) than ω_c . We notice from eq (63) that in both LPC and WC case $\langle u^2 \rangle_{Hi}$ are the same. But while in the WC case the two terms are of the same order $\langle u^2 \rangle_{Low} \simeq \langle u^2 \rangle_{Hi}$, in the LPC case $\langle u^2 \rangle_{Low} \ll \langle u^2 \rangle_{Hi}$ as far as the density increases (fig.3). This is due to the renormalization of the low energy frequencies. Therefore, the electronic fluctuation in the LPC increases more slowly with density than those of the WC. At given density, the electronic fluctuation of the WC is greater than those of the LPC and this fact explains the shifting of the quantum melting toward higher densities.

The cross-over is also evident in the polaron radius. In the upper panel of fig. 7 we plot the polaron radius as defined by the eq.(36). We see that for any value of the e-ph coupling, the polaron radius tends to decrease as far as the density is increased. We recall that as far as the renormalized plasma frequency eq.(2) exceeds the phonon frequency, we enter in a region in which the polarization is adiabatically slow compared to the electronic motion. Therefore, the electronic charge appears as a static distribution whose radius decreases upon increasing the density and the polaron radius follows this trend. The crossover is evident by scaling the polaron radius with r_s , as reported in the lower panel of fig.7 at intermediate and strong α .

It is possible to evaluate the high density limit of the radial distribution of the induced charge. The characteristic length $\ell^2(\tau)$ defined in eq. (39) is expressed in term of τ -dependent positional fluctuations $d(\tau)$ eq.(38) (imaginary time diffusion). As reported in Appendix C, $d(\tau)$ is an integral of a function $d_{s,\vec{k}}(\tau)$ weighted by the DOS $\rho(\omega)$ of the Wigner lattice.

To have an estimate of this integral we can evaluate the the function $d_{s,\vec{k}}(\tau)$ at a certain average frequency that we choose to be the highest density limit of the plasma frequency $\omega_P/\sqrt{\epsilon_\infty}$. At low temperature ($k_B T \ll \hbar\omega_P/\sqrt{\epsilon_\infty}$) we get the following estimate for $\ell^2(\tau)$

$$\ell^2(\tau) \simeq \frac{\hbar}{m\omega_P/\sqrt{\epsilon_\infty}} \left(1 - e^{-2\frac{\omega_P}{\sqrt{\epsilon_\infty}}\tau}\right) \quad (64)$$

with $0 < \tau < \beta/2$ [50].

The characteristic time scale of electronic diffusion in imaginary time is $\tau_{el} = (\omega_P/\sqrt{\epsilon_\infty})^{-1}$. Now in the polaron radius R_P of eq.(37) another time scale appears $\tau_{ph} = \omega_{LO}^{-1}$ but at high density $\tau_{ph} \gg \tau_{el}$.

Now we can separate in the imaginary time integral appearing in eq.(37) the lowest time scale τ_{el} contribution

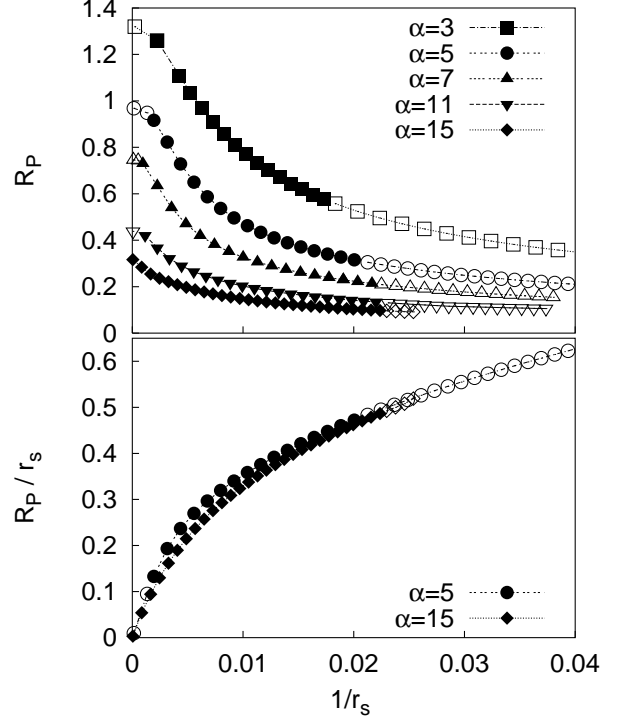


FIG. 7: Polaron radius in polaronic units (upper panel) and polaron radius scaled with r_s (lower panel) vs $(1/r_s)$ (a.u.) for different α in the case $\eta = 0.9$ at low temperature ($T = 5 \cdot 10^{-2}$ p.u.). Filled points refers to the solid phase.

and following the calculation reported in appendix E we get:

$$g(r) = \frac{1}{\epsilon} \left[\frac{r}{\frac{\hbar}{m\omega_{LO}}} \left(1 - \text{erf}\sqrt{\frac{r^2}{\langle u^2 \rangle}}\right) + \frac{2r^2}{\langle u^2 \rangle} \frac{e^{-\frac{r^2}{2\langle u^2 \rangle}}}{(2\pi \langle u^2 \rangle)^{3/2}} \right]. \quad (65)$$

The first term of eq. (65) takes into account quantum charge fluctuations which are relevant at small distances, while the remaining term is a classical contribution coming from the static charge distribution. Notice that only the first term depends on the e-ph interaction. Therefore, the polaron radius tends to the same high density asymptotic value for different values of the e-ph coupling α (see upper panel of fig.7).

d) High polarizability: softening of internal mode

This is the case in which the polarization gives a large contribution to the total interaction energy of the system. The system can be thought as being composed by interacting dipoles which are made by electrons surrounded by their polarization. Contrary to the low polarizability case, dipoles interact through both attractive and repul-

sive forces.

The cross-over region is now localized within liquid phase. To realize this, let us consider the condition $\omega_{P,H} \simeq \omega_{TO}$ which estimates a lower bound for the density cross-over. Using eq. (1) for $\omega_{P,H}$ and eq. (11) for α , we get for the crossover r_s^*

$$\frac{1}{r_s^{*3}} \frac{\alpha^4}{\eta(1-\eta)^4} = \text{const.} \quad (66)$$

From the previous estimate we see that as far as η approach unity the crossover moves toward low density eventually entering the solid phase. As far as we know from the discussion of fig. 5 the low polarizability strong coupling value of r_s^* ($1/r_1^* \simeq 0.0135$ for $\eta_1 = 0.90519$) the high polarizability crossover density can be determined by

$$\frac{1}{r_2^*} = \left(\frac{\eta_2}{\eta_1} \right)^{1/3} \left(\frac{1-\eta_2}{1-\eta_1} \right)^{4/3} \frac{1}{r_1^*} \quad (67)$$

that gives for $\eta_2 = 0.16667$ $1/r_2^* = 0.141$ that is in the liquid phase far from quantum melting (see fig.1).

Inside the solid phase, the expansion parameter $\epsilon_{s,\vec{k}}$ given by eq. (52) is small for all Wigner Crystal frequencies and for all e-ph coupling constants. Therefore, we are in the low density regime for any density inside the solid phase. The solutions of eqs.(53,54) can be taken as representative of the frequencies of the system as the electron fluctuation is given by the low density expansion eqs.(58,59), which holds for all energies.

For small and intermediate couplings, $\langle u^2 \rangle_-$ eq.(58) is the leading term in the mean electronic fluctuation of the dipolar model near the quantum melting. The optical polaron frequencies eq.(59) are negligible for the calculation of the fluctuation. In this case, the quantum melting density scales as eq.(46).

Now we discuss the case of strong e-ph coupling where we observe a saturation of the critical quantum melting density. In fig. 8 the electronic fluctuation is reported for $\alpha = 13$. Contrary to the small/intermediate coupling case, $\langle u^2 \rangle_+$ is now the leading term near the quantum melting. The melting density given by eq.(46) is not a good estimate due to the contribution of polaronic optical modes which is important at the quantum melting. The same scenario of ref.[27] is recovered: the optical polaronic frequencies drive the melting at strong coupling and high polarizability.

In fact in this regime the prefactor of eq. (59) $M/(M_T + m) \sim 1$ and $\mu \sim m$ since $M_T \gg m$ then $\langle u^2 \rangle_+ \sim \hbar/m\omega_{pol}$ when $k_B T \ll \hbar\omega_{pol}$.

In fig. 9 we see that ω_{pol} suffers a sudden drop as it is shown in fig.9. [27]. This softening induces an abrupt increase of electron fluctuation which is dominated by the term $\langle u^2 \rangle_+$ (see fig.8). In ref.[27], the same behavior for ω_{pol} is reported. Because ω_{pol} represents the internal

frequency of the individual dipoles, renormalized by the mean field of the others, this softening is due to the attractive term in the interaction between the polarons [27] [51]. We stress however that employing a more quantitative Lindemann criterion together with a self-consistent variational calculation of all Feynmans' parameter we get quantum melting in a region in which ω_{pol} did not actually soften. Another reason for that come for the explicit account for of the hetero-interactions in our scheme which as was noticed also in ref. [28] contributes to shift the softening toward higher densities. As a result the softening of internal polaronic frequency approaches quantum melting only asymptotically for large α . Notice at melting ω_{pol} still remains locked around its zero density value for $\alpha < 15$.

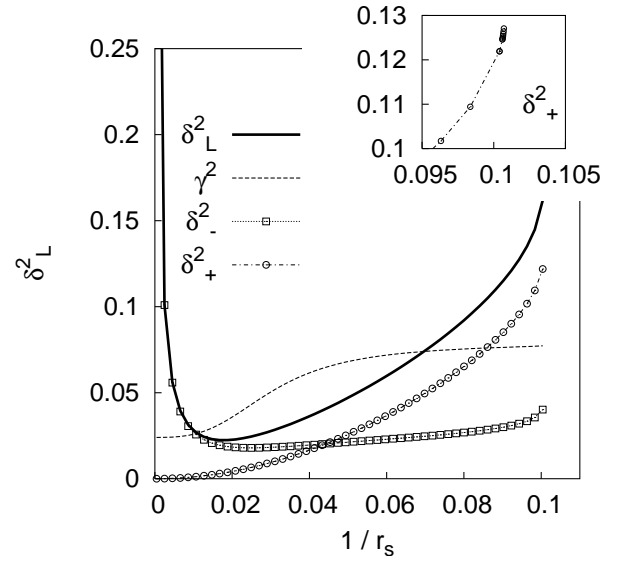


FIG. 8: The Lindemann ratio (solid line) and the function γ (dashed line) for $\eta = 0.17$ and $\alpha = 13$. $T = 1.10^{-5}$ (a.u.). Contributions δ_{\pm}^2 as in figure 3 d are also shown. The inset shows the abrupt slope increase of the term δ_+^2 (see also fig.9)

In fig. 10 we show the behavior of the polaron radius as a function of density. While in the solid phase it remains almost constant, when approaching the melting density it suddenly increases. This behavior can be understood by taking into account that the polaron radius is essentially determined by the diffusion in imaginary time of the electron path eqs.(36,37,38,39). Its maximum value occurs at $\tau = \beta/2$ which diverges at the softening of the polaronic frequency ($\omega_{pol} \sim 0$) (see appendix E). Polaronic clouds tends to overlap (fig.10 lower panel). However, the polaronic nature of each particle of the LPC is preserved up to quantum melting.

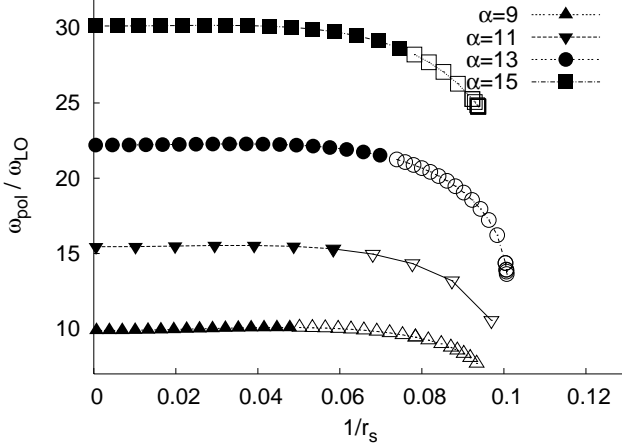


FIG. 9: The polaronic frequency vs $1/r_s$ (a.u.) for $\eta = 0.17$ at strong e-ph coupling α at low temperature ($T = 5.10^{-3}$ p.u.). Filled points refer to the solid phase.

2D CASE

The results obtained in the 2D case are qualitatively similar to the 3D case. Both the cross-over phenomenon in the low polarizability case and the softening of the polaronic frequency in the high polarizability case are observed. Results are reported in the zero temperature phase diagram of fig. 2. In this figure, we compare the phase diagrams in 2D and 3D by scaling appropriately the 2D e-ph coupling constant following the single polaron results of ref.[49]: $\alpha_{3D} = (3\pi/4)\alpha_{2D}$. 2D and 3D melting curves scale well according to the zero density scaling for all studied cases. A discrepancy is found in the the high polarizability strong e-ph coupling softening of ω_{pol} . Let us first discuss the scaling at finite density.

In our variational scheme, the DOS of the WC is the peculiar difference between the 2D and 3D cases. To see this explicitly let us compare the e-ph interaction terms $\mathcal{S}_{e-ph-e}^{self}$. Assuming polaronic units we get:

$$\frac{1}{\beta} \frac{\langle \mathcal{S}_{e-ph-e}^{self} \rangle_{T,3D}}{3N} = -(\alpha) \frac{\sqrt{2}}{6} \int_0^{\frac{\beta}{2}} d\tau \frac{D_o(\tau)}{\sqrt{\frac{\pi}{2} d_{3D}(\tau)}} \quad (68)$$

$$\frac{1}{\beta} \frac{\langle \mathcal{S}_{e-ph-e}^{self} \rangle_{T,2D}}{2N} = -\left(\frac{3\pi}{4}\alpha\right) \frac{\sqrt{2}}{6} \int_0^{\frac{\beta}{2}} d\tau \frac{D_o(\tau)}{\sqrt{\frac{\pi}{2} d_{2D}(\tau)}} \quad (69)$$

where the diffusion in imaginary-time $d(\tau)$ eq.(38) is itself a functional of the DOS. We notice from eqs.(68,69) that the free energy functional scales explicitly as in the single polaron case [49] by scaling the coupling constant α . Related to the different 2D and 3D DOS we remark the different behavior of the frequencies of the normal

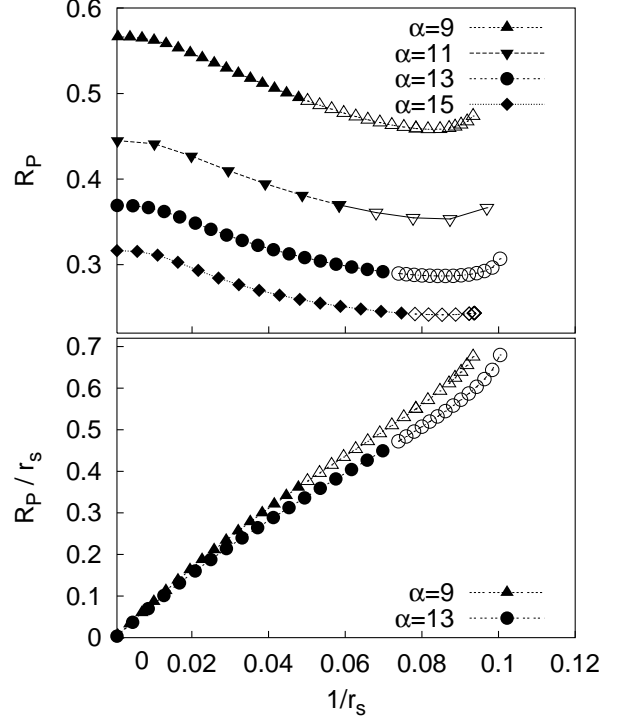


FIG. 10: Polaron radius in polaronic units (upper panel) and polaron radius scaled with r_s (lower panel) vs $(1/r_s)$ (a.u.) for different α and $\eta = 0.17$ at low temperature ($T = 5.10^{-3}$ p.u.). Filled points refer to the solid phase.

modes. Noticeably, the “optical” branches go to zero as $\sim \sqrt{k}$ at long wavelengths [47]. As in the 3D case, the frequencies of the LPC are splitted in four branches (fig.11) $\omega_{s,k}^{acu} \rightarrow \Omega_1 \Omega_3$ and $\omega_{s,k}^{opt} \rightarrow \Omega_2 \Omega_4$ according to the same equation of 3D eq.(47). The 2D value for ω_W comparing in eq.(47) is given in appendix B eq. (108).

Let us discuss the deviation from the the scaling at strong coupling, which we see from fig.2 in the density of the softening of the polaronic frequency ω_{pol} . Actually we observe that a steep fall of the variational parameter $v(r_s)$ occurs as density increases determining the softening of ω_{pol} eq.(48). Peculiar features of the DOS enters in the variational determination of $v(r_s)$ as can be achieved by the following argument. First of all we assume that w is very close to the value ω_{LO} at strong coupling. Then we notice that as in 3D high polarizability case the renormalized plasma frequency is much less than the phonon frequency and the discussion which follows eq. 52 holds for any density lower than critical density of the softening. In this case the spectrum is composed by the low energy branches (renormalized WC) and the by polaronic branches weakly dispersed around ($\sim v$) as eqs.(53,54) (see also fig.11). Using this results at low temperatures

($\beta \rightarrow \infty$), the condition for the extrema of \mathcal{F}_V reads:

$$1 - \frac{1}{v^{3/2}} \sqrt{\frac{\omega_p^2}{w\varepsilon_o}} \mathcal{M}_2 + g(\alpha, \eta, r_s, v) = 0 \quad (70)$$

where the first and second terms are the derivative of \mathcal{F}_T eq.(146) and g is the derivative of eqs.(147,148,149) from Appendix C. As $v(r_s) \rightarrow 0$ for $r_s \simeq r_c$ the second term acquires importance and DOS enters in the second moment \mathcal{M}_2 . However there are other terms which are divergent as $v \rightarrow 0$ coming from the explicit form of the function g .

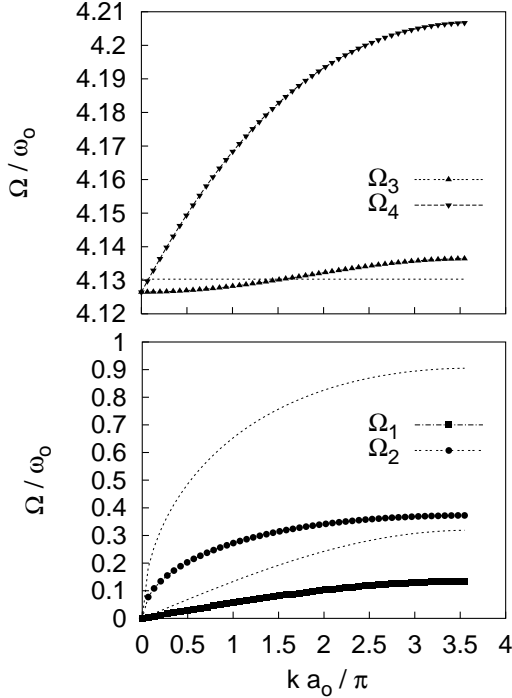


FIG. 11: 2D case. The eigenfrequencies of system along the direction (10) for $\eta = 0.9$ and $\alpha = 2.12$. $1/r_s = 8 \cdot 10^{-3}$ (a.u.), $T = 2.5 \cdot 10^{-5}$ (a.u.). Density is close to the classical liquid-solid transition. Upper panel: The frequencies of polaronic branch weakly dispersed around the polaronic frequency $\omega_{pol} \simeq v$ (dashed line). Lower panel: The renormalized Wigner crystal branches (points) and the pure WC branches (dashed lines).

CONCLUSIONS

We have studied the behavior of a low density electron gas in the presence of a polarizable medium, where polaronic effects may play a relevant role. To take quantum effects correctly into account both the quantum and the classical melting, we have used the generalized Lindemann criterion to determine the transition lines. Because

the amplitude of quantum fluctuations depends on the e-ph renormalized plasma frequency, the Lindemann rule has been critically re-examined and adapted to the polaron crystal. This procedure allows to determine quantitatively the phase diagram of the model and to extend the study of the model to the low polarizability case, which was not studied before. We have also studied the 2D case, showing that the dimensional dependence is not crucial to determine the nature of the quantum melting within in our harmonic variational scheme. The scaling predicted for the e-ph coupling constant at zero density do apply as well at non zero density up to quantum melting. A noticeable difference instead is in the position of the density of the softening of the polaronic frequency which in 3D is much closer to the melting than in 2D case. This suggests that the hetero-interactions are less effective to destabilize the dipolar crystal in 2D. However other possible mechanism, (lattice-effects, structural disorder or impurities) can cooperate to the localization together with the interactions between the electrons and lead to the formation of a pinned Wigner Crystal. In this case the melting can not be predicted by the Lindemann rule but a similar dipolar instability due to the long-range interaction between the electrons can still drives the melting.

While the weak e-ph coupling regime is similar for both low and high polarization case, the strong coupling scenario is qualitatively different. In the low polarizability regime, a crossover occurs inside the solid phase when the renormalized plasma frequency approaches the phonon frequency. At low density, we still have a LPC, while at higher densities the electron-phonon interaction is weakened irrespective of the bare electron-phonon coupling. In this case, polaron clouds overlap as and the polaron feature of the crystal is lost. This means that the high density electronic screening regime found by Mahan in the liquid phase [19] is here recovered in the solid phase at low density in our non-perturbative approach, for any value of the bare coupling α .

In the high polarizability regime, we have recovered the incipient instability which was found in previous studies near the solid phase [26, 27] and also in the liquid phase [28]. In comparison with previous work, we have found that this regime is restricted to very large values of the coupling $\alpha > 10$ leaving an interesting intermediate region of coupling in which polarons may exist in the liquid phase. This region can in principle be explored with non perturbative numerical techniques as e.g. Path Integral Monte Carlo. Work along this direction is currently in progress.

Finally we notice that our low polarizability scenario of density crossover inside the solid phase bear some resemblance to that found for ripplonic polaron systems [52]. Though the electron-ripplon interaction in this system is different from the Fröhlich type, resonances in the absorption spectrum observed by Grimes and Adams [54],

their explanation at low density [55] relies on the same qualitative arguments developed in the present work. Recent works on high density ripplonic polaron systems realized on a helium bubbles predicts also in this case a mixing between plasmon and polaron modes [56].

The general result that e-ph interaction effects can stabilize the Wigner crystal phase could motivate experimental studies on two dimensional electronic devices or heterostructures involving polarizable media.

ACKNOWLEDGMENTS

Authors acknowledge S. Fratini and P. Quemerais for useful discussions and critical reading of the manuscript. We thanks also J. Lorenzana for useful suggestions. One of us (G.R.) thanks the also the kind hospitality of CNRS-LEPES Grenoble were a part of this work has been done.

This work was supported by MIUR-Cofin 2001 and MIUR-Cofin 2003 matching funds programs.

APPENDIX A: THE LOW ENERGY CUT OFF IN 2D

The 2D DOS can defined as

$$\rho(\omega) = \sum_{s=1,2} \int_{V_B} d^2k \delta(\omega - \omega_{s,k}) \quad (71)$$

where V_B is the volume of the first Brillouin's zone (1BZ). Let us consider a small fraction ε of the plasma frequency ω_P . At long wavelength ($k = 0$), we have the 2D dispersion laws for the acoustical mode is $\omega_1(k) \simeq c_1 k$ while the "optical" $\omega_2(k) \simeq c_2 \sqrt{k}$ [41]. As a consequence the behavior of the DOS for $\omega \simeq 0$ is

$$\int_0^{2\pi} d\theta \int_0^{k(\varepsilon)} dk k \delta(\omega - c_1 k) = \frac{2\pi}{c_1^2} \omega \quad (72)$$

$$\int_0^{2\pi} d\theta \int_0^{k(\varepsilon)} dk k \delta(\omega - c_2 \sqrt{k}) = \frac{4\pi}{c_2^4} \omega^3 \quad (73)$$

Introducing the scaled frequency x defined as $\omega = \omega_P x$ and the quantum parameter η_q eq.(25) the thermal electronic fluctuation is expressed as an average on the DOS as

$$\langle u^2 \rangle = \frac{\hbar}{m} \left\langle \frac{\coth(\eta_q x)}{x} \right\rangle_{DOS} \quad (74)$$

$$\langle \dots \rangle_{DOS} = \int dx \dots \rho(\omega_P x) \quad (75)$$

$$\frac{\coth(\eta_q x)}{x} = \frac{1}{\eta_q x^2} + \eta_q \left[\alpha_0 + \alpha_2 (\eta_q x)^2 + \dots \right] \quad (76)$$

Since $\rho(\omega_P x) \sim x$ for $x \rightarrow 0$, the average in eqs. (74) converges for any of x^{2n} with $n \geq 0$ in the the expansion

eq.(76). In the $n = 0$ term we consider infrared cut-off x_c giving

$$\left\langle \frac{1}{x^2} \right\rangle \simeq \int_{x_c}^{\varepsilon} dx \frac{(2\pi/c_1^2)\omega_P}{x} + \int_{\varepsilon} dx \frac{\rho(\omega_P x)}{x^2} \quad (77)$$

$$\simeq \frac{2\pi\omega_P}{c_1^2} \ln\left(\frac{\varepsilon}{x_c}\right) + \int_{\varepsilon} dx \frac{\rho(\omega_P x)}{x^2}. \quad (78)$$

This term diverges logarithmically as $x_c \rightarrow 0$. However ($\eta_q \rightarrow \infty$) as we approach the quantum region. The electronic fluctuation turns out to be cut-off independent if

$$\left\langle \frac{1}{x^2} \right\rangle \ll \eta_q^2 \left\langle \alpha_0 + \alpha_2 (\eta_q x)^2 + \dots \right\rangle. \quad (79)$$

We have chosen for the cut-off frequency $x_c = \omega_{min}/\omega_P \simeq 5 \cdot 10^{-5}$ so that the condition eq.(79) is fulfilled around $\eta_q(T, r_s) \geq 10$ which corresponds to a large region inside to the solid phase.

By the relation for acoustical long wave excitation $\omega_{min} = c_1 k_{min}$ and $k_{min} = 2\pi / (r_s \sqrt{N})$, the number of electrons is $N = 5.24 \cdot 10^6$. Our inverse second moment of DOS is $\mathcal{M}_{-2} = 12.5$ (cfr ref. [48] $\mathcal{M}_{-2} = 8.16$ for $N = 1024$).

APPENDIX B: THE HARMONIC VARIATIONAL APPROXIMATION

We expand in the harmonic approximation the terms $\mathcal{S}_{e-e}, \mathcal{S}_{e-J}, \mathcal{S}_{e-ph-e}^{dist}$ (eqs.6,9,8) of the effective electron action \mathcal{S}_{eff} eq.(4). Let $\vec{r}_i = \vec{R}_i + \vec{u}_i$ where \vec{R}_i is the lattice point of the crystal and \vec{u}_i is the electronic displacement from \vec{R}_i . The differences between vectors are expressed as $\Delta \vec{u}_{i,j}(\tau, \sigma) = \vec{u}_j(\sigma) - \vec{u}_i(\tau)$ and $\vec{R}_{j,i} = \vec{R}_j - \vec{R}_i$. We separate the static terms from the dynamical ones

$$\mathcal{S}_{e-J} = \mathcal{S}_{e-J}^o + \Delta \mathcal{S}_{e-J} \quad (80)$$

$$\mathcal{S}_{e-e} = \mathcal{S}_{e-e}^o + \Delta \mathcal{S}_{e-e} \quad (81)$$

$$\mathcal{S}_{e-ph-e}^{dist} = \mathcal{S}_{e-ph-e}^{o,dist} + \Delta \mathcal{S}_{e-ph-e}^{dist} \quad (82)$$

The static terms are

$$\mathcal{S}_{e-J}^o = \beta \frac{e^2}{\varepsilon_0} \int d^D r \left[- \sum_i \frac{\rho_J}{|\vec{R}_i - \vec{r}|} + \int d^D r' \frac{\rho_J^2/2}{|\vec{r}' - \vec{r}|} \right] \quad (83)$$

$$\mathcal{S}_{e-e}^o = \beta \frac{e^2}{2\varepsilon_\infty} \sum_{i \neq j} \frac{1}{|\vec{R}_{j,i}|} \quad (84)$$

$$\begin{aligned} \mathcal{S}_{e-ph-e}^{o,dist} &= - \frac{e^2 \omega_{LO}}{4\bar{\varepsilon}} \sum_{i \neq j} \frac{\int_0^\beta d\tau \int_0^\beta d\sigma D_o(\tau - \sigma)}{|\vec{R}_{j,i}|} \\ &= - \beta \frac{e^2}{2\bar{\varepsilon}} \sum_{i \neq j} \frac{1}{|\vec{R}_{j,i}|} \end{aligned} \quad (85)$$

At a given point of the lattice labeled by the index i the sum on $j \neq i$ for the all three term $\mathcal{S}_{e-J}^o, \mathcal{S}_{e-e}^o, \mathcal{S}_{e-ph-e}^{o,dist}$ goes to zero. Therefore the presence of the retarded hetero-interaction $\mathcal{S}_{e-ph-e}^{dist}$ due to e-ph coupling is necessary for the stability of the Wigner crystal in a polarizable medium ($\varepsilon_0 \neq \varepsilon_\infty$). Moreover since

$$\mathcal{S}_{e-e}^o + \mathcal{S}_{e-J}^o + \mathcal{S}_{e-ph-e}^{o,dist} = \mathcal{S}_{WC}^o / \varepsilon_0 \quad (86)$$

the e-ph interaction does not change the equilibrium positions of the pure electronic crystal (WC) which corresponds to the minimum of the potential energy.

The sum of the dynamical parts gives

$$\begin{aligned} \mathcal{S}_{dyn} &= \Delta \mathcal{S}_{e-J} + \Delta \mathcal{S}_{e-e} + \Delta \mathcal{S}_{e-ph-e}^{dist} \\ &= \int_0^\beta d\tau \left[\sum_i V_J(\vec{u}_i(\tau)) + \sum_i V_{e-e}(\vec{u}_i(\tau)) \right] \end{aligned} \quad (87)$$

$$V_J(\vec{u}_i(\tau)) = -\frac{e^2 \rho_J}{\varepsilon_0} \int d^D r \left(\frac{1}{|\vec{u}_i(\tau) - \vec{r}|} - \frac{1}{r} \right) \quad (88)$$

$$V_{e-e}(\vec{u}_i(\tau)) = \frac{e^2}{2} \sum_{\vec{R}_j, j \neq i} \int_0^\beta d\sigma F(\tau - \sigma) U_{j,i}(\sigma, \tau) \quad (89)$$

$$U_{j,i}(\sigma, \tau) = \frac{1}{|\vec{R}_{j,i} + \Delta \vec{u}_{i,j}(\sigma, \tau)|} - \frac{1}{|\vec{R}_{j,i}|} \quad (90)$$

$$F(\tau - \sigma) = \frac{\delta(\tau - \sigma)}{\varepsilon_\infty} - \frac{\omega_{LO}}{2\varepsilon} D_o(\tau - \sigma) \quad (91)$$

From now we drop on the double σ, τ indexes in $\Delta \vec{u}_{i,j}$. Expanding $U_{j,i}$ eq.(90) in the harmonic approximation $\Delta \vec{u}_{i,j} \ll \vec{R}_{j,i}$, we have

$$U_{j,i}^H(\sigma, \tau) = -\frac{\Delta \vec{u}_{i,j} \cdot \vec{R}_{j,i}}{R_{j,i}^3} + \frac{1}{2} \Delta \vec{u}_{i,j} \cdot \vec{\mathcal{I}}(\vec{R}_{j,i}) \Delta \vec{u}_{i,j} \quad (92)$$

and eq.(89) becomes

$$V_{e-e}^H(\vec{u}_i(\tau)) = \frac{e^2}{2} \sum_{\vec{R}_j, j \neq i} \int_0^\beta d\sigma F(\tau - \sigma) U_{j,i}^H(\sigma, \tau) \quad (93)$$

$\vec{\mathcal{I}}_{\alpha\beta}(\vec{R}_{j,i})$ is given by

$$[\vec{\mathcal{I}}_j]_{\alpha\beta} = \frac{\delta_{\alpha\beta}}{[\vec{R}_j - \vec{R}_i]^3} - 3 \frac{[\vec{R}_j - \vec{R}_i]_\alpha [\vec{R}_j - \vec{R}_i]_\beta}{[\vec{R}_j - \vec{R}_i]^5} \quad (94)$$

In V_{e-e}^H eq. (93), the linear terms of eq.(92) ($\sim \Delta \vec{u}_{i,j} \cdot \vec{R}_{j,i}$) give no contribution to \mathcal{S}_{dyn} eq.(87) by definition of equilibrium configuration (minimum extreme of potential energy).

To evaluate the integral V_J eq. (88) and the sums on index j in V_{e-e}^H eq. (93), we consider a sphere S_R of radius R (a disk in 2D) centered on site i . The interaction of

i -th electron with the jellium and with all electrons inside S_R is given by

$$V_J^R(\vec{u}_i(\tau)) = -\frac{e^2 \rho_J}{\varepsilon_0} \int_{S_R} d^D r \left(\frac{1}{|\vec{u}_i(\tau) - \vec{r}|} - \frac{1}{r} \right) \quad (95)$$

$$V_{e-e}^{R,H}(\vec{u}_i(\tau)) = \frac{e^2}{2} \sum_{\substack{j \neq i \\ R_{j,i} < R}} \int_0^\beta d\sigma F(\tau - \sigma) U_{j,i}^H(\sigma, \tau) \quad (96)$$

To obtain the full harmonic potential we first perform the limit $R \rightarrow \infty$ of eqs.(95,96) and then we sum on index i in eq. (87).

3D case

By Gauss's law (with the condition $V_J^R(0) = 0$), we have for eq.(95)

$$V_J^R(\vec{u}_i(\tau)) = \frac{1}{2} m \omega_W^2 |\vec{u}_i(\tau)|^2 \quad (97)$$

where the Wigner frequency is $\omega_W^2 = \omega_P^2/3$. Because of V_J^R is independent of the size of S_R , eq.(95) does not change in the limit $R \rightarrow \infty$.

We have to evaluate the following sums in eq.(96).

$$\sum_{\substack{j \neq i \\ R_{j,i} < R}} U_{j,i}^H(\sigma, \tau) = \frac{1}{2} \sum_{\substack{j \neq i \\ R_{j,i} < R}} \Delta \vec{u}_{i,j} \cdot \vec{\mathcal{I}}(\vec{R}_{j,i}) \Delta \vec{u}_{i,j} \quad (98)$$

Reminding that $\Delta \vec{u}_{i,j} = \vec{u}_i - \vec{u}_j$ we have two diagonal $((i, i) \text{ and } (j, j))$ two off-diagonal $((i, j) \text{ and } (j, i))$ terms in eq. (98).

A diagonal term can explicitly written as

$$\frac{1}{2} \vec{u}_i \left(\sum_{\substack{j \neq i \\ R_{j,i} < R}} \vec{\mathcal{I}}(\vec{R}_{j,i}) \right) \vec{u}_i = \vec{u}_i(\tau) \vec{\mathcal{D}} \vec{u}_i(\tau) \quad (99)$$

the other diagonal term give the same contribution as can be easily check if we firstly we carry on the limit $R \rightarrow \infty$ and then the sum on index i and j . The symmetric matrix $\vec{\mathcal{D}}$ entering in eq. (99) is defined as sum of the matrices $\vec{\mathcal{I}}(\vec{R}_j)$ eq.(94) on b.c.c. lattice points \vec{R}_j inside S_R . By the cubic symmetry, the diagonal terms are equal $\vec{\mathcal{D}}_{XX} = \vec{\mathcal{D}}_{YY} = \vec{\mathcal{D}}_{ZZ}$ (rotation of $(\pi/2)$ around x,y,z axis) so that

$$\vec{\mathcal{D}}_{\alpha\alpha} = \sum_{\substack{j \neq i \\ R_{j,i} < R}} \frac{\vec{\mathcal{I}}_{XX}(\vec{R}_{j,i}) + \vec{\mathcal{I}}_{YY}(\vec{R}_{j,i}) + \vec{\mathcal{I}}_{ZZ}(\vec{R}_{j,i})}{3} = 0 \quad (100)$$

and the diagonal terms vanishes.

The off-diagonal element also vanishes using a reflection symmetry with respect to planes $x, y, z = 0$

$$\sum_{\substack{j \neq i \\ R_{j,i} < R}} \frac{X_{\alpha,j} X_{\beta,j}}{R_{j,i}^5} = - \sum_{\substack{j \neq i \\ R_{j,i} < R}} \frac{X_{\alpha,j} X_{\beta,j}}{R_{j,i}^5} \quad (101)$$

therefore

$$\sum_{\substack{j \neq i \\ R_{j,i} < R}} \frac{X_{\alpha,j} X_{\beta,j}}{R_j^5} = 0 \quad (102)$$

Lastly inserting the two off-diagonal $((i, j)$ and $(j, i))$ terms of eq. (98) in eq.(96), taking the limit $R \rightarrow \infty$ and summing on index i , we obtain the term $(\sum_i V_{e-e}(u_i))$ of eq.87

$$\begin{aligned} & \sum_i \lim_{R \rightarrow \infty} V_{e-e}^{R,H}(\vec{u}_i(\tau)) = \\ &= -\frac{e^2}{4} \sum_i \sum_{j \neq i} \int_0^\beta d\sigma F(\tau - \sigma) \vec{u}_i \cdot \vec{\mathcal{I}}(\vec{R}_{j,i}) \vec{u}_j \\ &- \frac{e^2}{4} \sum_i \sum_{j \neq i} \int_0^\beta d\sigma F(\tau - \sigma) \vec{u}_j \cdot \vec{\mathcal{I}}(\vec{R}_{j,i}) \vec{u}_i \\ &= \frac{e^2}{2} \sum_i \sum_{j \neq i} \int_0^\beta d\sigma F(\tau - \sigma) \vec{u}_j(\sigma) \vec{\mathcal{I}}(\vec{R}_{j,i}) \vec{u}_i(\tau) \end{aligned} \quad (103)$$

Summing eqs.(97,103) we obtain the terms $\mathcal{S}_{e-J}^H, \mathcal{S}_{e-e}^H, \mathcal{S}_{e-ph-e}^{H,dist}$ eqs.(21,22) of the harmonic variational action \mathcal{S}_T eq.(19).

2D case

In 2D the interaction potential $V_J^R(u)$ of a uniform positive charged disk of radius R eq. (95) is

$$V_J^R(u) = -\frac{e^2 \rho_J}{\epsilon_0} \int_0^{2\pi} d\theta F(\theta) \quad (104)$$

where

$$F(\theta) = A(u) - u - R + u \cos(\theta) \ln \frac{R - u \cos(\theta) + A(u)}{u(1 - \cos(\theta))}$$

and

$$A(u) = \sqrt{R^2 + u^2 - 2Ru \cos(\theta)}. \quad (105)$$

In the limit $(u/R) \rightarrow 0$, we have

$$V_J^R(\vec{u}_i) = \frac{e^2}{\epsilon_0} \rho_J \frac{\pi}{R_S} u_i^2 \quad (106)$$

in the limit $R \rightarrow \infty$ we have $V_J^R(\vec{u}_i) = 0$ since the total electric field of an infinite charged disk is perpendicular to the disk.

Then we have to evaluate the sums eq.98 as in 3D case. The two off-diagonal $((i, j)$ and $(j, i))$ terms of eq. (98) gives the identical result eq.103 of the 3D case.

As in 3D case the diagonal term (i, i) of eq.98 is written as eq.99 where the matrix \mathcal{D} in 2D is defined as sum of

the matrices $\vec{\mathcal{I}}(\vec{R}_j)$ eq.(94) on hexagonal lattice points \vec{R}_j . Contrary to the 3D case, the matrix \mathcal{D} is not zero in 2D case. By the lattice symmetry, the off-diagonal elements are zero while the diagonal terms are equal to

$$\overline{\mathcal{D}}_{\alpha\alpha} = \frac{1}{2} \sum_{\substack{j \neq i \\ R_{j,i} < R}} \frac{R_j^2 - 3X_j^2}{R_j^5} + \frac{R_j^2 - 3Y_j^2}{R_j^5} = - \sum_{\substack{j \neq i \\ R_{j,i} < R}} \frac{1}{2R_j^3} \quad (107)$$

As definition 2D Wigner frequency we use

$$\omega_W^2 = \frac{e^2}{m} \lim_{R \rightarrow \infty} \sum_{\substack{j \neq i \\ R_{j,i} < R}} \frac{1}{2R_{j,i}^3} \quad (2D) \quad (108)$$

For an hexagonal lattice of nearest neighbor distance $d_{n.n.}$, we have $\sum_{j \neq i} (1/2R_{j,i}^3) = 5.51709/d_{n.n.}^3$. Then the local potential which acts on each electrons is expressed as

$$V_{2D}(\vec{u}_i(\tau)) = \frac{1}{2} m \omega_W^2 |\vec{u}_i(\tau)|^2 \quad (109)$$

As in 3D case summing eqs.(103,109) we obtain the terms $\mathcal{S}_{e-J}^H, \mathcal{S}_{e-e}^H, \mathcal{S}_{e-ph-e}^{H,dist}$ eqs.(21,22) of the harmonic variational action \mathcal{S}_T eq.(19).

Normal modes

The normal modes are defined as

$$\vec{u}_i = \frac{1}{\sqrt{N}} \sum_{\vec{k},s} \hat{\epsilon}_{\vec{k},s} q_{\vec{k},s} e^{i\vec{k} \cdot \vec{R}_i} \quad (110)$$

where the vectors \vec{k} belongs to the 1BZ of the reciprocal lattice, $\hat{\epsilon}_{\vec{k},s}$ are eigenvector with eigenvalue $\omega_{\vec{k},s}^2$ of the dynamical matrix $\overline{\mathcal{M}}$ which is defined as

$$\overline{\mathcal{M}}_{\alpha\beta} = \delta_{\alpha\beta} \omega_W^2 + \frac{e^2}{m} \sum_{\vec{R}_i \neq 0} \vec{\mathcal{I}}_{\alpha\beta}(\vec{R}_i) e^{i\vec{k} \cdot \vec{R}_i} \quad (111)$$

We have shown that eq.(111) takes also the form in 2D case

$$\overline{\mathcal{M}}_{\alpha\beta} = \frac{e^2}{m} \sum_{\vec{R}_i \neq 0} \vec{\mathcal{I}}_{\alpha\beta}(\vec{R}_i) \left(e^{i\vec{k} \cdot \vec{R}_i} - 1 \right) \quad (112)$$

By using the Ewald's transformations it is possible to demonstrate that eq.(111) and eq.(112) are also equivalent in 3D case .

By definition of $\hat{\epsilon}_{\vec{k},s}$ and $\overline{\mathcal{M}}$ eq.(111), the following properties holds

$$\hat{\epsilon}_{\vec{k}',s'} \overline{\mathcal{M}} \hat{\epsilon}_{\vec{k},s} = \omega_{\vec{k},s}^2 \hat{\epsilon}_{\vec{k}',s'} \cdot \hat{\epsilon}_{\vec{k},s} = \omega_{\vec{k},s}^2 \delta_{\vec{k},\vec{k}'} \delta_{s,s'} \quad (113)$$

$$\frac{m}{e^2} \hat{\epsilon}_{\vec{k}',s'} [\overline{\mathcal{M}} - \delta_{\alpha\beta} \omega_W^2] \hat{\epsilon}_{\vec{k},s} = \frac{m}{e^2} \left(\omega_{\vec{k},s}^2 - \omega_W^2 \right) \delta_{\vec{k},\vec{k}'} \delta_{s,s'} \quad (114)$$

moreover

$$\sum_{i, \text{lat.}} e^{i(\vec{k}-\vec{k}') \cdot \vec{R}_i} = \delta_{\vec{k}, \vec{k}'} \quad (\forall \vec{k} \in 1\text{BZ}) \quad (115)$$

From eqs.(110-115) we have the following identities

$$\sum_i |\dot{\vec{u}}_i(\tau)|^2 = \sum_{s, \vec{k}} |\dot{q}_{\vec{k}, s}(\tau)|^2 \quad (116)$$

$$\sum_i |\vec{u}_i(\tau)|^2 = \sum_{s, \vec{k}} |q_{\vec{k}, s}(\tau)|^2 \quad (117)$$

$$\sum_i \vec{u}_i(\tau) \cdot \vec{u}_i(\sigma) = \sum_{s, \vec{k}} q_{\vec{k}, s}^*(\tau) q_{\vec{k}, s}(\sigma) \quad (118)$$

$$\sum_i |\vec{u}_i(\tau) - \vec{u}_i(\sigma)|^2 = \sum_{s, \vec{k}} |q_{\vec{k}, s}(\tau) - q_{\vec{k}, s}(\sigma)|^2 \quad (119)$$

$$\sum_{i \neq j} \vec{u}_i(\tau) \vec{u}_j(\sigma) = \sum_{s, \vec{k}} \frac{\omega_{\vec{k}, s}^2 - \omega_W^2}{e^2/m} q_{\vec{k}, s}(\tau) q_{\vec{k}, s}^*(\sigma) \quad (120)$$

Inserting eqs.(116-120) in eqs.(18,20,21,22) we obtain the harmonic variational action \mathcal{S}_T eq. (19) expressed in terms of the WC normal modes

$$\mathcal{S}_T = \sum_{s, \vec{k}} \int_0^\beta d\tau L_{s, k}(\tau) \quad (121)$$

where the Lagrangian is

$$\begin{aligned} L_{s, k} = & \frac{1}{2} m \left| \dot{q}_{\vec{k}, s}(\tau) \right|^2 + \frac{1}{2} m \frac{\omega_{\vec{k}, s}^2}{\varepsilon_0} \left| q_{\vec{k}, s}(\tau) \right|^2 \\ & + \frac{m w (v^2 - w^2)}{8} \int_0^\beta d\sigma D_V(\tau - \sigma) \left| q_{\vec{k}, s}(\tau) - q_{\vec{k}, s}(\sigma) \right|^2 \\ & + \frac{m \omega_{LO} (\omega_{\vec{k}, s}^2 - \omega_W^2)}{8\varepsilon} \int_0^\beta d\sigma D_o(\tau - \sigma) \left| q_{\vec{k}, s}(\tau) - q_{\vec{k}, s}(\sigma) \right|^2 \end{aligned} \quad (122)$$

APPENDIX C: THE VARIATIONAL FREE ENERGY \mathcal{F}_V

The first term of the variational free energy \mathcal{F}_V eq. (23) is the free energy \mathcal{F}_T associated to the partition function of the trial action \mathcal{Z}_T . This is calculated as the functional integral eq.(3) where \mathcal{S}_{eff} eq. (4) is replaced by \mathcal{S}_T eq. (19). The second term of \mathcal{F}_V is the mean value eq. (14) of the difference between $\mathcal{S}_{e-ph-e}^{self}$ eq. (7) and \mathcal{S}_{Feyn} eq. (18).

We start by changing the dynamical variables of integration from $\{\vec{u}_i(\tau)\}$ to $\{q_{s, \vec{k}}(\tau)\}$. By reality condition we have $q_{-\vec{k}, s} = q_{\vec{k}, s}^*$ and $\hat{\varepsilon}_{-\vec{k}, s} = -\hat{\varepsilon}_{\vec{k}, s}$, therefore we must sum only \vec{k} vectors in the upper half space ($k_z > 0$) of 1BZ

$$\vec{u}_i = \frac{1}{\sqrt{N}} \sum_{s, \vec{k}, k_z > 0} \hat{\varepsilon}_{\vec{k}, s} \left[q_{\vec{k}, s} e^{i\vec{k} \cdot \vec{R}_i} - q_{\vec{k}, s}^* e^{-i\vec{k} \cdot \vec{R}_i} \right] \quad (123)$$

Therefore the real and imaginary part of $q_{s, \vec{k}}$ for all k with ($k_z > 0$) of the 1BZ are the actual independent variables.

$$\begin{pmatrix} \vec{u}_1 \\ \vec{u}_2 \\ \dots \\ \vec{u}_{N-1} \\ \vec{u}_N \end{pmatrix} = \begin{pmatrix} U_{\vec{k}_1, s_1}^{1, x_1} & \dots & U_{\vec{k}_{N/2}, s_D}^{1, x_1} \\ \dots & \dots & \dots \\ \dots & \dots & \dots \\ \dots & \dots & \dots \\ U_{\vec{k}_1, s_1}^{N, x_D} & \dots & U_{\vec{k}_{N/2}, s_D}^{N, x_D} \end{pmatrix} \begin{pmatrix} \text{Re} \left(q_{\vec{k}_1, 1} \right) \\ \text{Im} \left(q_{\vec{k}_1, 1} \right) \\ \dots \\ \dots \\ \text{Re} \left(q_{\vec{k}_{N/2}, s} \right) \\ \text{Im} \left(q_{\vec{k}_{N/2}, s} \right) \end{pmatrix} \quad (124)$$

where

$$U_{\vec{k}_\ell, s}^{\alpha} = \frac{1}{\sqrt{N}} \left(\hat{\varepsilon}_{\vec{k}_\ell, s} \right)_\alpha \begin{pmatrix} \cos(\vec{k}_\ell \cdot \vec{R}_i) \\ \sin(\vec{k}_\ell \cdot \vec{R}_i) \end{pmatrix} \quad (125)$$

By eqs.(113,115) the Jacobian of transformation eq.(124) is $J = 2^{DN}$. Therefore

$$\begin{aligned} \mathcal{Z}_T &= \int \prod_i \mathcal{D}[\vec{u}_i(\tau)] e^{-\mathcal{S}_T} \\ &= \int \prod_{s, \vec{k}, k_z > 0} \mathcal{D}[q_{s, \vec{k}}^{Re}(\tau)] \mathcal{D}[q_{s, \vec{k}}^{Im}(\tau)] e^{-\mathcal{S}_T} \end{aligned} \quad (126)$$

where \mathcal{S}_T is expressed in terms of the normal modes eqs. (121,122).

Using the periodicity condition ($q_{s, \vec{k}}(0) = q_{s, \vec{k}}(\beta)$), we have the following Fourier expansion

$$q_{s, \vec{k}}(\tau) = q_{s, \vec{k}, c} + \delta q_{s, \vec{k}}(\tau) \quad (127)$$

$$q_{s, \vec{k}, c} = \frac{1}{\beta} \int_0^\beta d\tau q_{s, \vec{k}}(\tau) \quad (128)$$

$$\delta q_{s, \vec{k}}(\tau) = \sum_{\substack{n=-\infty \\ n \neq 0}}^{\infty} q_{s, \vec{k}, n} e^{i\omega_n \tau} \quad (129)$$

$$q_{s, \vec{k}, n} = \frac{1}{\beta} \int_0^\beta d\tau q_{s, \vec{k}}(\tau) e^{-i\omega_n \tau} \quad (\omega_n = \frac{2\pi}{\beta} n) \quad (130)$$

where we have separated the mean value eq.(128) of path on the imaginary time from the fluctuation around it eq.(129). The action (eqs.121,122) is quadratic in $\{q_{s, \vec{k}}(\tau)\}$ and eq.(126) can be separated into two terms

$$\mathcal{Z}_{T, c} = \int \prod_{s, \vec{k}, k_z > 0} \frac{dq_{s, \vec{k}, c}^{Re} dq_{s, \vec{k}, c}^{Im}}{\pi \hbar^2 / m k_B T} e^{-\mathcal{S}_T^c \{q_{s, \vec{k}, c}\}} \quad (131)$$

$$\mathcal{Z}_{T, \delta q} = \int \prod_{\substack{n \neq 0 \\ s, \vec{k}, k_z > 0}} \frac{dq_{s, \vec{k}, n}^{Re} dq_{s, \vec{k}, n}^{Im}}{\pi k_B T / m \omega_n^2} e^{-\delta \mathcal{S}_T \{\delta q_{s, \vec{k}}(\tau)\}} \quad (132)$$

For the kinetic term of the lagrangian eq.(122) we have

$$\frac{1}{2} m \int_0^\beta d\tau |\dot{q}_{s, \vec{k}}|^2 = \beta m \sum_{n \neq 0} \omega_n^2 |q_{s, \vec{k}, n}|^2. \quad (133)$$

While the harmonic term of eq.(122) gives

$$\begin{aligned} \frac{1}{2}m\frac{\omega_{\vec{k},s}^2}{\varepsilon_0}\int_0^\beta d\tau |q_{\vec{k},s}(\tau)|^2 &= \beta\frac{m\omega_{\vec{k},s}^2}{2\varepsilon_0}|q_{\vec{k},s,c}|^2 \\ &+ \beta m\sum_{n\neq 0}\frac{\omega_{\vec{k},s}^2}{\varepsilon_0}|q_{s,\vec{k},n}|^2 \end{aligned} \quad (134)$$

The Feynman's variational term of eq.(122) reads

$$\begin{aligned} \frac{mw(v^2 - w^2)}{8}\int_0^\beta d\tau \int_0^\beta d\sigma D_V(\tau - \sigma) |\delta q_{\vec{k},s}(\tau) - \delta q_{\vec{k},s}(\sigma)|^2 \\ = \beta m\sum_{n\neq 0}\frac{(v^2 - w^2)\omega_n^2}{\omega_n^2 + w^2}|q_{\vec{k},s,n}|^2. \end{aligned} \quad (135)$$

And the last term of the eq.(122) gives

$$\begin{aligned} \frac{m\omega_{LO}(\omega_{\vec{k},s}^2 - \omega_W^2)}{8\varepsilon}\int_0^\beta d\tau \int_0^\beta d\sigma D_o(\tau - \sigma) |\delta q_{\vec{k},s}(\tau) - \delta q_{\vec{k},s}(\sigma)|^2 \\ = \beta m\sum_{n\neq 0}\frac{(\omega_{\vec{k},s}^2 - \omega_W^2)\omega_n^2}{\varepsilon(\omega_n^2 + \omega_{LO}^2)}|q_{s,\vec{k},n}|^2 \end{aligned} \quad (136)$$

performing the gaussian integrals eqs.(131,132) give

$$\begin{aligned} \mathcal{Z}_{T,c} &= \int \prod_{s,\vec{k},k_z>0} \frac{dq_{\vec{k},s,c}^{Re} dq_{\vec{k},s,c}^{Im}}{\pi\hbar^2/mk_BT} e^{-\frac{m}{k_BT}\frac{|q_{\vec{k},s,c}|^2}{\omega_{s,\vec{k}}^2/\varepsilon_0}} \\ &= \prod_{s,\vec{k}} \frac{k_BT}{\hbar\omega_{s,\vec{k}}/\sqrt{\varepsilon_0}} \end{aligned} \quad (137)$$

$$\begin{aligned} \mathcal{Z}_{T,\delta q} &= \int \prod_{n\neq 0} \frac{dq_{\vec{k},s,n}^{Re} dq_{\vec{k},s,n}^{Im}}{\pi k_BT/m\omega_n^2} e^{-\frac{m}{k_BT}\frac{|q_{\vec{k},s,n}|^2}{\lambda_{s,\vec{k},n}}}} \\ &= \prod_{n\neq 0} \omega_n^2 \lambda_{s,\vec{k},n} \end{aligned} \quad (138)$$

where

$$\frac{1}{\lambda_{s,\vec{k},n}} = \omega_n^2 + \frac{(v^2 - w^2)\omega_n^2}{\omega_n^2 + w^2} + \frac{\omega_{\vec{k},s}^2}{\varepsilon_0} + \frac{(\omega_{\vec{k},s}^2 - \omega_W^2)\omega_n^2}{\varepsilon(\omega_n^2 + \omega_{LO}^2)} \quad (139)$$

We now introduce the frequencies Ω_γ^2 , ($\gamma = 1, 2, 3$) as the opposite of the roots of cubic

$$\begin{aligned} \mathcal{P}_3(z) &= z^3 + a_2 z^2 + a_1 z + a_0 \\ a_2 &= v^2 + \omega_{LO}^2 + \frac{\omega_{\vec{k},s}^2}{\varepsilon_0} + \frac{\omega_{\vec{k},s}^2 - \omega_W^2}{\varepsilon} \\ a_1 &= \omega_{LO}^2 v^2 + \frac{\omega_{\vec{k},s}^2}{\varepsilon_0}(\omega_{LO}^2 + w^2) + w^2 \frac{\omega_{\vec{k},s}^2 - \omega_W^2}{\varepsilon} \\ a_0 &= \frac{\omega_{LO}^2 w^2 \omega_{\vec{k},s}^2}{\varepsilon_0} \end{aligned} \quad (140)$$

so that

$$\lambda_{s,\vec{k},n} = \frac{(\omega_n^2 + \omega_{LO}^2)(\omega_n^2 + w^2)}{(\omega_n^2 + \Omega_1^2)(\omega_n^2 + \Omega_2^2)(\omega_n^2 + \Omega_3^2)} \quad (141)$$

$$= \sum_{\gamma=1}^3 \frac{A_\gamma}{\omega_n^2 + \Omega_\gamma^2} \quad (142)$$

$$A_1 = \frac{(\Omega_1^2 - \omega_{LO}^2)(\Omega_1^2 - w^2)}{(\Omega_1^2 - \Omega_2^2)(\Omega_1^2 - \Omega_3^2)} \quad (\text{cyclic perm. } \gamma = 1, 2, 3) \quad (143)$$

$$\lambda_{s,\vec{k},0} = \sum_{\gamma=1}^3 \frac{A_\gamma}{\Omega_\gamma^2} = \frac{\omega_{LO}^2 w^2}{(\Omega_1^2)(\Omega_2^2)(\Omega_3^2)} = \frac{1}{\omega_{\vec{k},s}^2/\varepsilon_0} \quad (144)$$

The gaussian integrals eq.(138) are convergent if $\lambda_{s,\vec{k},n}$ are positive numbers $\forall(s, \vec{k}, n)$. This condition is fulfilled if Ω_γ^2 of eq.(141) are *all* positive. The numerical minimization of the variational free energy has been made enforcing this constraint.

Using eq.(141) in eq.(138) we have

$$\begin{aligned} \mathcal{Z}_{T,\delta q} &= \prod_{n\neq 0} \frac{\omega_n^2(\omega_n^2 + \omega_{LO}^2)(\omega_n^2 + w^2)}{(\omega_n^2 + \Omega_1^2)(\omega_n^2 + \Omega_2^2)(\omega_n^2 + \Omega_3^2)} \\ &= \prod_{n\neq 0} \frac{(\omega_n^2 + \omega_{LO}^2)(\omega_n^2 + w^2)}{\omega_n^2} \prod_{\gamma} \frac{\omega_n^2}{\omega_n^2 + \Omega_{\gamma,s,\vec{k}}^2} \end{aligned}$$

where

$$\begin{aligned} \prod_{n\neq 0} \frac{(\omega_n^2 + \omega_{LO}^2)}{\omega_n^2} &= \left(\frac{\sinh(\hbar\omega_{LO}/2k_BT)}{\hbar\omega_{LO}/2k_BT} \right)^{DN} \\ \prod_{n\neq 0} \frac{(\omega_n^2 + w^2)}{\omega_n^2} &= \left(\frac{\sinh(\hbar w/2k_BT)}{\hbar w/2k_BT} \right)^{DN} \\ \prod_{n\neq 0} \frac{\omega_n^2}{\omega_n^2 + \Omega_{\gamma,s,\vec{k}}^2} &= \prod_{s,\vec{k},\gamma} \frac{\hbar\Omega_{\gamma,s,\vec{k}}/2k_BT}{\sinh(\hbar\Omega_{\gamma,s,\vec{k}}/2k_BT)} \end{aligned}$$

and finally

$$\begin{aligned} \mathcal{F}_{T/N} &= -Dk_BT \ln \left[\sinh \left(\frac{\hbar\omega_{LO}}{2k_BT} \right) \sinh \left(\frac{\hbar w}{2k_BT} \right) \right] \\ &+ k_BT \frac{1}{N} \sum_{s,\vec{k},\gamma} \ln \sinh \left(\frac{\hbar\Omega_{\gamma,s,\vec{k}}}{2k_BT} \right) \end{aligned} \quad (145)$$

We can substitute the sum on (\vec{k}_i, s) with the integral on the WC DOS $\rho(\omega)$ having

$$\begin{aligned} \mathcal{F}_{T/N} &= -Dk_BT \ln \left[\sinh \left(\frac{\hbar\omega_{LO}}{2k_BT} \right) \sinh \left(\frac{\hbar w}{2k_BT} \right) \right] \\ &+ Dk_BT \int d\omega \rho(\omega) \sum_{\gamma=1}^3 \ln \sinh \left(\frac{\hbar\Omega_\gamma(\omega)}{2k_BT} \right) \end{aligned} \quad (146)$$

The mean value of $\mathcal{S}_{e-ph-e}^{self}$ eq. (7) in 3D is now

$$\begin{aligned}
& \langle \mathcal{S}_{e-ph-e}^{self} \rangle_{T,3D}/N = \\
& = -\frac{\omega_{L0}e^2}{4\bar{\epsilon}N} \int \int_0^\beta d\tau d\sigma D_o(\tau - \sigma) \sum_i \left\langle \frac{1}{|\vec{u}_i(\tau) - \vec{u}_i(\sigma)|} \right\rangle_T \\
& = -\frac{\omega_{L0}e^2}{4\bar{\epsilon}} \int \int_0^\beta d\tau d\sigma D_o(\tau - \sigma) \int \frac{d^3q}{(2\pi)^3} \frac{4\pi}{q^2} \left\langle e^{i\vec{q} \cdot [\vec{u}_i(\tau) - \vec{u}_i(\sigma)]} \right\rangle_T \\
& = -\frac{\omega_{L0}e^2}{4\bar{\epsilon}} \int \int_0^\beta d\tau d\sigma D_o(\tau - \sigma) \int \frac{d^3q}{(2\pi)^3} \frac{4\pi}{q^2} e^{-\frac{1}{2}d_{3D}(\tau - \sigma)q^2} \\
& = -\frac{\omega_{L0}e^2}{4\bar{\epsilon}} \int \int_0^\beta d\tau d\sigma \frac{D_o(\tau - \sigma)}{\sqrt{\frac{\pi}{2}d_{3D}(\tau - \sigma)}} \\
& = -2\beta \frac{\omega_{L0}e^2}{4\bar{\epsilon}} \int_0^{\frac{\beta}{2}} d\tau \frac{D_o(\tau)}{\sqrt{\frac{\pi}{2}d_{3D}(\tau)}}
\end{aligned}$$

while in 2D ($q^2 = q_\perp^2 + q_z^2$)

$$\begin{aligned}
& \langle \mathcal{S}_{e-ph-e}^{self} \rangle_{T,2D}/N = \\
& = -\frac{\omega_{L0}e^2}{4\bar{\epsilon}} \int \int_0^\beta d\tau d\sigma D_o(\tau - \sigma) \int \frac{d^3q}{(2\pi)^3} \frac{4\pi}{q^2} e^{-\frac{1}{2}d_{2D}(\tau - \sigma)q^2} \\
& = -\frac{\omega_{L0}e^2}{4\bar{\epsilon}} \int \int_0^\beta d\tau d\sigma D_o(\tau - \sigma) \int \frac{d^2q_\perp}{(2\pi)^2} \frac{2\pi}{q_\perp} e^{-\frac{1}{2}d_{2D}(\tau - \sigma)q_\perp^2} \\
& = -\frac{\omega_{L0}e^2}{4\bar{\epsilon}} \int \int_0^\beta d\tau d\sigma \frac{(\pi/2)D_o(\tau - \sigma)}{\sqrt{\frac{\pi}{2}d_{2D}(\tau - \sigma)}} \\
& = -2\beta \left(\frac{\pi}{2}\right) \frac{\omega_{L0}e^2}{4\bar{\epsilon}} \int_0^{\frac{\beta}{2}} d\tau \frac{D_o(\tau)}{\sqrt{\frac{\pi}{2}d_{2D}(\tau)}}
\end{aligned} \tag{148}$$

The mean value of \mathcal{S}_{Feyn} eq. (18) is

$$\begin{aligned}
& \langle \mathcal{S}_{Feyn} \rangle_T/N = \\
& = -D \frac{mw(v^2 - w^2)}{8} \int \int_0^\beta d\tau d\sigma D_T(\tau - \sigma) d_D(\tau - \sigma)
\end{aligned} \tag{149}$$

To obtain eqs.(147,148,149) we have used

$$\left\langle e^{i\vec{q} \cdot [\vec{u}_i(\tau) - \vec{u}_i(\sigma)]} \right\rangle_{T,D} = e^{-\frac{1}{2}d_D(\tau - \sigma)q^2} \tag{150}$$

where $d_D(\tau - \sigma)$ is the imaginary time diffusion in the LPC defined in eq.(38)

$$\begin{aligned}
& d(\tau) = \\
& = \frac{1}{ND} \sum_{s,k} \frac{\hbar}{m} \sum_\gamma \frac{A_\gamma}{\Omega_\gamma^2} \frac{2 \sinh \frac{\Omega_\gamma \tau}{2} \sinh \left[\frac{\hbar \Omega_\gamma}{2k_B T} (1 - \tau/\beta) \right]}{\sinh \frac{\hbar \Omega_\gamma}{2k_B T}}
\end{aligned} \tag{151}$$

We will demonstrate eqs.(150,151) in the next subsection.

Calculation of $\langle \exp(i\vec{q} \cdot [\vec{u}_i(\tau) - \vec{u}_i(\sigma)]) \rangle_T$

From eqs.(110,129) we have

$$i\vec{q} \cdot [\vec{u}_i(\tau) - \vec{u}_i(\sigma)] = \sum_{\substack{s,k,z>0 \\ n \neq 0}} \left[q_{\vec{k},s,n} J_{s,k,n}^*(\tau - \sigma, \vec{q}) + \text{c.c.} \right] \tag{152}$$

$$J_{s,k,n}^*(\tau - \sigma, \vec{q}) = \frac{i}{\sqrt{N}} \vec{q} \cdot \hat{\epsilon}_{\vec{k},s} (e^{i\omega_n \tau} - e^{i\omega_n \sigma}) e^{i\vec{k} \cdot \vec{R}_i} \tag{153}$$

using eq.(132) we have

$$\begin{aligned}
& \langle \exp(i\vec{q} \cdot [\vec{u}_i(\tau) - \vec{u}_i(\sigma)]) \rangle_T = \\
(147) & = \frac{1}{Z_{T,\delta q}} \prod_{\substack{n \neq 0 \\ s,\vec{k},k_z>0}} \frac{dq_{\vec{k},s,n}^{Re}}{\pi k_B T / m \omega_n^2} \frac{dq_{\vec{k},s,n}^{Im}}{\pi k_B T / m \omega_n^2} e^{-\delta S_T \{ \delta q_{s,\vec{k}}(\tau) \}} e^{i\vec{q} \cdot [\vec{u}_i(\tau) - \vec{u}_i(\sigma)]} \\
& = \frac{1}{Z_{T,\delta q}} \prod_{\substack{n \neq 0 \\ s,\vec{k},k_z>0}} \frac{dq_{\vec{k},s,n}^{Re}}{\pi k_B T / m \omega_n^2} \frac{dq_{\vec{k},s,n}^{Im}}{\pi k_B T / m \omega_n^2} e^{-\frac{m}{k_B T} \frac{|q_{\vec{k},s,n}|^2}{\lambda_{s,\vec{k},n}} + q_{\vec{k},s,n} J_{\vec{k},s,n}^* + \text{c.c.}} \\
& = \prod_{\substack{n \neq 0 \\ s,\vec{k},k_z>0}} e^{-\frac{k_B T}{m} \lambda_{s,\vec{k},n} |J_{\vec{k},s,n}|^2} = e^{-\frac{1}{2}d_D(\tau - \sigma)q^2}
\end{aligned} \tag{154}$$

where

$$\begin{aligned}
d_D(\tau - \sigma) & = \frac{2k_B T}{mNq^2} \sum_{s,\vec{k}} \left| \vec{q} \cdot \hat{\epsilon}_{\vec{k},s} \right|^2 \sum_{n \neq 0} \lambda_{s,\vec{k},n} [1 - \cos(\omega_n \tau)] \\
& = \frac{2k_B T}{mN} \sum_{s,\vec{k}} \left| \hat{q} \cdot \hat{\epsilon}_{\vec{k},s} \right|^2 \sum_{n \neq 0} \lambda_{s,\vec{k},n} [1 - \cos(\omega_n \tau)] \\
& = \frac{1}{N} \sum_{s,k} \left| \hat{q} \cdot \hat{\epsilon}_{\vec{k},s} \right|^2 d_{\omega_{s,k}}(\tau - \sigma)
\end{aligned} \tag{155}$$

the component of frequency $\omega_{s,k}$ of the imaginary time diffusion $d_D(\tau - \sigma)$ is

$$\begin{aligned}
d_{\omega_{s,k}}(\tau - \sigma) & = \frac{2k_B T}{m} \sum_{n \neq 0} \lambda_{s,\vec{k},n} [1 - \cos(\omega_n \tau)] \\
& = \frac{2k_B T}{m} \sum_\gamma A_\gamma \sum_{n \neq 0} \frac{(1 - \cos(\omega_n \tau))}{\omega_n^2 + \Omega_\gamma^2} \\
& = \frac{\hbar}{m} \sum_\gamma \frac{A_\gamma}{\Omega_\gamma^2} \frac{2 \sinh \frac{\Omega_\gamma \tau}{2} \sinh \left[\frac{\hbar \Omega_\gamma}{2k_B T} (1 - \tau/\beta) \right]}{\sinh \frac{\hbar \Omega_\gamma}{2k_B T}}
\end{aligned} \tag{156}$$

Now we demonstrate that

$$\sum_{s,k} \left| \hat{q} \cdot \hat{\epsilon}_{\vec{k},s} \right|^2 d_{\omega_{s,k}}(\tau - \sigma) = \frac{1}{D} \sum_{s,k} d_{\omega_{s,k}}(\tau - \sigma) \tag{157}$$

$$\sum_{s,k} d_{\omega_{s,k}} \left| \hat{q} \cdot \hat{\epsilon}(\vec{k},s) \right|^2 = \sum_{s,k} d_{\omega_{s,k}} \sum_{\alpha,\beta=1,D} \hat{q}_\alpha \hat{q}_\beta \hat{\epsilon}_\alpha(\vec{k},s) \hat{\epsilon}_\beta(\vec{k},s)$$

for $(\alpha = \beta)$ we have

$$\begin{aligned} \sum_{s,k} d_{\omega_{s,k}} \sum_{\alpha=1,D} \hat{q}_\alpha^2 \hat{\epsilon}_\alpha^2(\vec{k}, s) &= \sum_{\alpha=1,D} \hat{q}_\alpha^2 \sum_{s,k} d_{\omega_{s,k}} \hat{\epsilon}_\alpha^2(\vec{k}, s) \\ &= \sum_{\alpha=1,D} \hat{q}_\alpha^2 \frac{1}{D} \sum_{s,k} d_{\omega_{s,k}} \\ &= \frac{1}{D} \sum_{s,k} d_{\omega_{s,k}} \end{aligned}$$

in fact all the sums $\sum_{s,k} d_{\omega_{s,k}} \hat{\epsilon}_\alpha^2(\vec{k}, s)$ give the same contribution, while the following sums are vanishing

$$\sum_{s,k} d_{\omega_{s,k}} \hat{\epsilon}_x \hat{\epsilon}_y = \sum_{s,k} d_{\omega_{s,k}} \hat{\epsilon}_x \hat{\epsilon}_z = \sum_{s,k} d_{\omega_{s,k}} \hat{\epsilon}_y \hat{\epsilon}_z = 0$$

To see explicitly this let us consider a reflection with respect to the plane $y = 0$, the function $d_{\omega_{s,k}}$ does not change because $\omega(s, k_x, k_y, k_z) = \omega(s, k_x, -k_y, k_z)$ and the sum $\sum_{s,k} d_{\omega_{s,k}} \hat{\epsilon}_x \hat{\epsilon}_y$ is not changed due the lattice symmetry

$$(\hat{\epsilon}_x, \hat{\epsilon}_y, \hat{\epsilon}_z) = (\hat{\epsilon}_x, -\hat{\epsilon}_y, \hat{\epsilon}_z)$$

and

$$\sum_{s,k} d_{\omega_{s,k}} \hat{\epsilon}_x \hat{\epsilon}_y = - \sum_{s,k} d_{\omega_{s,k}} \hat{\epsilon}_x \hat{\epsilon}_y$$

Therefore the sum is vanishes.

APPENDIX D: MEAN ELECTRONIC FLUCTUATION

The relation between the mean electronic fluctuation and the imaginary time diffusion $d_D(\tau)$ eq.(38) is

$$\begin{aligned} d(\tau) &= \frac{\langle |\vec{u}(\tau) - \vec{u}|^2 \rangle_T}{D} \\ &= \frac{2}{D} \left[\langle |\vec{u}(0)|^2 \rangle - \langle \vec{u}(\tau) \cdot \vec{u}(0) \rangle \right] \end{aligned}$$

We can express $d_D(\tau)$ using eq.(151) as

$$\begin{aligned} d(\tau) &= \\ &= \frac{1}{ND} \sum_{s,k} \frac{\hbar}{m} \sum_{\gamma} \frac{A_\gamma}{\Omega_\gamma^2} \frac{\cosh(\beta\Omega_\gamma/2) - \cosh(\Omega_\gamma[\beta/2 - \tau])}{\sinh(\beta\Omega_\gamma)} \end{aligned}$$

we have

$$\frac{\langle |\vec{u}|^2 \rangle}{D} = \int d\omega \rho(\omega) \sum_{\gamma} \frac{\hbar A_\gamma(\omega)}{2m\Omega_\gamma^2(\omega)} \coth\left(\frac{\beta\Omega_\gamma(\omega)}{2}\right) \quad (158)$$

then the Lindemann's ratio $\langle |\vec{u}|^2 \rangle / d_{n.n.}^2$ can be calculated using

$$d_{n.n.}^2 = \frac{3}{4} \left(\frac{8\pi}{3} \right)^{2/3} r_s^2 \quad (3D: bcc) \quad (159)$$

$$d_{n.n.}^2 = \frac{2\pi}{\sqrt{3}} r_s^2 \quad (2D: hex) \quad (160)$$

APPENDIX E: CORRELATION FUNCTIONS

We now calculate the self term C_1^{self} eq. (34). We assume that the equilibrium position of the reference electron $i = 1$ is the origin ($\vec{R}_1 = 0$). Using

$$\langle \exp(i\vec{u}_i \vec{q}) \rangle_T = \exp(-\sigma_T^2 q^2 / 2) \quad \sigma_T^2 = \langle u^2 \rangle_T / D$$

where σ_T^2 is the thermal mean quadratic fluctuation, the density distribution $\rho_1(\vec{r})$ is given by

$$\langle \hat{\rho}_1(\vec{r}) \rangle_T = \int \frac{d^D q}{(2\pi)^D} e^{i\vec{q}\vec{r}} \langle e^{i\vec{u}_1 \vec{q}} \rangle_T = \frac{e^{-r^2/2\sigma_T^2}}{(2\pi\sigma_T^2)^{D/2}} \quad (161)$$

The self term is

$$\begin{aligned} &\langle \rho_1(\vec{r}) \rho_1(\vec{r}', \tau) \rangle_T = \\ &= \int \frac{d^D q}{(2\pi)^D} \int \frac{d^D q'}{(2\pi)^D} \langle e^{i\vec{q}(\vec{u}_1 - \vec{r})} e^{i\vec{q}'(\vec{u}_1(\tau) - \vec{r}')} \rangle_T \\ &= \int \frac{d^D q}{(2\pi)^D} \int \frac{d^D q'}{(2\pi)^D} e^{-i\vec{q}\vec{r}} e^{i\vec{q}'(\vec{r} - \vec{r}')} \langle e^{-i\vec{q}\vec{u}_1} e^{i\vec{q}'(\vec{u}_1(\tau) - \vec{u}_1)} \rangle_T \\ &= \int \frac{d^D q}{(2\pi)^D} \int \frac{d^D q'}{(2\pi)^D} e^{-i\vec{q}\vec{r}} e^{i\vec{q}'(\vec{r} - \vec{r}')} e^{-\frac{\sigma_T^2}{2} q^2} e^{-\frac{d(\tau)}{2} \vec{q}' \cdot [\vec{q}' + \vec{q}]} \\ &= \langle \hat{\rho}_1(\vec{r}) \rangle_T \frac{e^{-\frac{|\vec{r} - \vec{r}' + \frac{d(\tau)}{2\sigma_T^2} \vec{r}'|^2}}{(2\pi\ell^2(\tau))^{D/2}} \end{aligned} \quad (162)$$

where $\ell^2(\tau)$ is given by eqs.(38,39).

Due to the term $(d(\tau)/2\sigma^2)\vec{r}'$, we notice that $\langle \rho_1(\vec{r}) \rho_1(\vec{r}', \tau) \rangle_T$ does not depend only on the relative distance $\vec{r}' - \vec{r}$ but also from the distance of electron from its localization position in the crystal. We assume $\vec{r} = 0$ (electron in its lattice point) and then we obtain eq.(35) in 3D and 2D case

$$g(r) = \frac{\pi(2r)^{D-1}}{\bar{\epsilon}} \frac{\omega_{LO}}{2} \int_0^\beta d\tau D_o(\tau) \frac{e^{-r^2/2\ell^2(\tau)}}{(2\pi\ell^2(\tau))^{3/2}} \quad (163)$$

then we obtain the polaron radius eq.(37) by eq.(36).

$$\text{Calculation of } \langle \exp(-i\vec{q}\vec{u}_1) \exp(i\vec{q}'(\vec{u}_1(\tau) - \vec{u}_1)) \rangle_T$$

Now we demonstrate the identity that we have used to obtain eq.162

$$\langle e^{-i\vec{q}\vec{u}_1} e^{i\vec{q}'(\vec{u}_1(\tau) - \vec{u}_1)} \rangle_T = e^{-\frac{\sigma_T^2}{2} q^2} e^{-\frac{d(\tau)}{2} \vec{q}' \cdot [\vec{q}' + \vec{q}]} \quad (164)$$

By eqs.(110,129) we have

$$\begin{aligned} &-i\vec{q}\vec{u}_1 + i\vec{q}'(\vec{u}_1(\tau) - \vec{u}_1) = \\ &= \sum_{\substack{s,k,z>0 \\ n \neq 0}} \frac{i}{\sqrt{N}} \hat{\epsilon}_{s,\vec{k}} \left[\vec{q}' (e^{i\omega_n \tau} - 1) - \vec{q} \right] q_{\vec{k},s,n} + \text{c.c.} \end{aligned}$$

As in eqs.(152,153,154), we obtain

$$\begin{aligned}
& \left\langle e^{-i\vec{q}\vec{u}_1} e^{i\vec{q}'(\vec{u}_1(\tau)-\vec{u}_1)} \right\rangle_T = \\
& = \exp \left(- \sum_{\substack{s, k_z > 0 \\ n \neq 0}} \frac{k_B T}{Nm} \sum_{\gamma} \frac{A_{\gamma}}{\omega_n^2 + \Omega_{\gamma}^2} \left| \hat{\varepsilon} \left[\vec{q}'(e^{\omega_n \tau} - 1) - \vec{q} \right] \right|^2 \right) \\
& = \exp \left(- \frac{\sigma^2}{2} q^2 \right) \exp \left(- \frac{d(\tau)}{2} \vec{q}' \left[\vec{q}' - \vec{q} \right] \right) \quad (165)
\end{aligned}$$

High density limit

The characteristic length $\ell^2(\tau)$ defined in eq.(39) is expressed in term of τ -dependent positional fluctuations eq.(38). At high density the typical frequency of the electronic fluctuations in the crystal is $\omega_P/\sqrt{\varepsilon_{\infty}}$ eq. (63).

Therefore to obtain an estimate of the integrals eqs.(155,156) which define $d_D(\tau)$, we can use a single frequency DOS of frequency $\omega_P/\sqrt{\varepsilon_{\infty}}$.

$$d_D(\tau) \simeq \frac{\hbar}{m \frac{\omega_P}{\sqrt{\varepsilon_{\infty}}}} \frac{\left(1 - e^{-\frac{\omega_P}{\sqrt{\varepsilon_{\infty}}} \tau}\right) \left(1 - e^{-\frac{\omega_P}{\sqrt{\varepsilon_{\infty}}} (\beta - \tau)}\right)}{1 - e^{-\frac{\omega_P}{\sqrt{\varepsilon_{\infty}}} \beta}}. \quad (166)$$

At low temperature ($k_B T \ll \hbar \omega_P/\sqrt{\varepsilon_{\infty}}$) we have

$$\langle u^2 \rangle_T \simeq \frac{\hbar}{2m \frac{\omega_P}{\sqrt{\varepsilon_{\infty}}}} \quad (167)$$

$$d_D(\tau) \simeq \frac{\hbar}{m \frac{\omega_P}{\sqrt{\varepsilon_{\infty}}}} \left(1 - e^{-\frac{\omega_P}{\sqrt{\varepsilon_{\infty}}} \tau}\right). \quad (168)$$

Then from eq.(39) we obtain $\ell^2(\tau)$ eq.(64). The rising-time is $\tau_{el} = 1/(2\omega_P/\sqrt{\varepsilon_{\infty}})$. Therefore we have approximately

$$\begin{aligned}
\ell^2(\tau) & \simeq \frac{\hbar}{m} \tau \quad (\tau \ll \tau_{el}) \\
\ell^2(\tau) & \simeq \frac{\hbar}{2m \frac{\omega_P}{\sqrt{\varepsilon_{\infty}}}} \quad (\tau \gg \tau_{el})
\end{aligned}$$

then we divide the integral in imaginary time appearing in eq.(36) according to the time scale τ_{el} so that we can approximate the integral in eq.(36) as

$$\begin{aligned}
\int_0^{\tau_{el}} d\tau D_o(\tau) \frac{e^{-r^2/2\ell^2(\tau)}}{(2\pi\ell^2(\tau))^{3/2}} & \simeq D_o(0) \int_0^{\tau_{el}} d\tau \frac{e^{-r^2/2\ell^2(\tau)}}{(2\pi\ell^2(\tau))^{3/2}} \\
& = \frac{m}{2\pi\hbar} \frac{1}{r} \left(1 - \text{erf} \sqrt{\frac{r^2}{\langle u^2 \rangle}}\right) \\
\int_{\tau_{el}}^{\beta} d\tau D_o(\tau) \frac{e^{-r^2/2\ell^2(\tau)}}{(2\pi\ell^2(\tau))^{3/2}} & \simeq \frac{e^{-r^2/2 \frac{\hbar}{m \frac{\omega_P}{\sqrt{\varepsilon_{\infty}}}}}}{(2\pi \langle u^2 \rangle)^{3/2}} \int_{\tau_{el}}^{\beta} d\tau D_o(\tau) \\
& \simeq \frac{e^{-r^2/2 \langle u^2 \rangle}}{(2\pi \langle u^2 \rangle)^{3/2}}.
\end{aligned}$$

Collecting these results we get eq. (65).

-
- [1] E. Wigner, Phys. Rev. **46**, 1002 (1934).
 - [2] Jongsoo Yoon, C. C. Li, D. Shahar, D. C. Tsui and M. Shayegan Phys. Rev. Lett. **82**, 1744 (1998).
 - [3] D. M. Ceperley, M. D. Jones, Phys. Rev. Lett. **76** 4572 (1996).
 - [4] B. Bernu, L. Cândido D. M. Ceperley, Phys. Rev. Lett. **86**, 870 (2001).
 - [5] S. T. Chui, B. Tanatar, Phys. Rev. Lett. **74**, 458 (1995).
 - [6] *Polarons and Excitons*, C. G. Kuper and G. D. Whitfield edits. (Oliver and Boyd, Edinburgh, 1962).
 - [7] *Polarons in Ionic Crystals and Polar semiconductor* (edition par. J. Devreese, Amsterdam, North Holland, 1972).
 - [8] A. Mooradian, G. B. Wright Phys. Rev. Lett. **16**, 999 (1966).
 - [9] B. Varga Phys. Rev. A **137**, 1896 (1965).
 - [10] G. Irmer, M. Wenzel, J. Monecke Phys. Rev. B **56**, 9524 (1997) and refs. therein.
 - [11] Y. H. Kim, C. M. Foster, A. J. Heeger, S. Cox and G. Stucky, Phys. Rev. B **38**, 6478 (1988).
 - [12] C. Taliani, R. Zambone, G. Raum, F. C. Matocotta and K. I. Pokhadnya, Solid State Commun. **66**, 487 (1988).
 - [13] S. Lupi, P. Calvani, M. Capizzi, P. Maselli, W. Sadowski and E. Walker, Phys. Rev. B **45**, 12470 (1992); P. Calvani, M. Capizzi, S. Lupi, P. Maselli, A. Paolone and P. Roy, Phys. Rev. B **53**, 2756 (1996).
 - [14] A. Lanzara, P. V. Bogdanov, X. J. Zhou, S. A. Kellar, D. L. Feng, E. D. Lu, T. Yoshida, H. Eisaki, A. Fujimori, K. Kishio, J. -I. Shimoyama, T. Noda, S. Uchida, Z. Hussain and Z. X. Shen, Nature **412**, 510-514 (2001).
 - [15] S. Fratini, P. Quémerais, Mod. Phys. Lett. B **12** 1003 (1998).
 - [16] M. A. Kastner, R. J. Birgeneau, G. Shirane, Y. Endoh, Rev. Mod. Phys. **70** p.897 (1998).
 - [17] I. Fedorov, J. Lorenzana, P. Dore, G. De Marzi, P. Maselli, P. Calvani, Phys. Rev. B **60** 11875 (1999).
 - [18] A. Lucarelli, S. Lupi, M. Ortolani, P. Calvani, H. Eisaki, N. Kikugawa, T. Fujita, M. Fujita, and K. Yamada Phys. Rev. Lett. **90**, 037002 (2003).
 - [19] A. V. Puchkov, T. Timusk, M. A. Karlow, S. L. Cooper, P. D. Han, D. A. Payne Phys. Rev. B **54** 6686 (1996).
 - [20] G. D. Mahan, *Many-Particle physics*, (Plenum, New York 1981) chap. 6; G. D. Mahan, in ref. [7] p.553.
 - [21] L. F. Lemmens, J. T. Devreese, F. Brosens Phys. stat. sol. (b) **82**, 439 (1977).
 - [22] G. Iadonisi, G. Capone, V. Cataudella, G. De Filippis Phys. Rev. B **53** 13497 (1996).
 - [23] I. Bozovic Phys. Rev. B **48**, 876 (1993).
 - [24] G. De Filippis, V. Cataudella, G. Iadonisi Eur. Phys. J. **8** 339 (1999).
 - [25] T. D. Lee, F. Low, D. Pines, Phys. Rev. **90**, 297 (1953).
 - [26] P. Quémerais Mod. Phys. Lett. B **9**, 1665 (1995).
 - [27] S. Fratini, P. Quémerais, Eur. Phys. J. B **14**, 99 (2000).
 - [28] S. Fratini, P. Quémerais, Eur. Phys. J. B **29**, 41 (2002).
 - [29] J. Lorenzana, Europhys. Lett. **53**, 532 (2001).
 - [30] p.29-80 of ref. [6]
 - [31] W. J. Carr Phys. Rev. **122** 1437 (1961).
 - [32] R. P. Feynman, A. R. Hibbs *Quantum Mechanics and Path Integrals* (McGraw-Hill, 1965).

- [32] R. T. Senger, A. Erelebi, Phys. Rev. B **60** p.10070 (1999).
- [33] R. P. Feynman, Phys. Rev. **97**, 660 (1955).
- [34] T. D. Schultz, Phys. Rev. **116**, 526 (1969).
- [35] R. Mochkovitch, J. P. Hansen Phys. Lett. **73 A** n.1, p.35 (1979).
- [36] Hitose Nagara, Yoichi Nagata and Tuto Nakamura, Phys. Rev. A **36** n.4, p.1859 (1987). (See footnote num. 31).
- [37] see ref. [4] (private communications for the value of interpolating parameter A for γ).
- [38] Notice however that this discussion does not involve the l.h.s. of eq.(24) in which ω_P appears as a result of harmonic approximation.
- [39] S. Ciuchi, J. Lorenzana , C. Pierleoni Phys. Rev. B **62**, 4426 (2000).
- [40] N. D. Mermin, Phys. Rev. **176**, 250 (1968).
- [41] L. Bonsall, A. A. Maradudin, Phys. Rev. B **15**, 1959 (1977).
- [42] R. A. Coldwell-Horsfall, A. A. Maradudin, J. of Mathematical Physics **1**, 395 (1960).
- [43] R. E. Peierls, Helv. Phys. Acta **7** (suppl.2) 81 (1936). (see also) *Quantum theory of solids* (par 3.3), Oxford University Press (1955).
- [44] L. D. Landau, E. M. Lifshitz, *Statistical physics*, Pergamon Press N. Y. (1968).
- [45] M. Baus, J. of Statistical Physics bf **22**, n.1 (1980).
- [46] A. Alastuey B. Jancovici, J. of Statistical Physics **24**, n.3 (1981).
- [47] R. S. Crandall, Phys. Rev. A **8**, 2136 (1973).
- [48] R. C. Gann S. Chakravarty G. V. Chester, Phys. Rev. B **20**, 326 (1979).
- [49] F. M. Peeters , J. T. Devreese Phys. Rev. B **36**, 4442 (1987).
- [50] Notice that $\ell^2(\tau)$ and $d(\tau)$ are symmetric function respect to time $\beta/2$ in the interval $0 < \tau < \beta$ as $D_o(\tau)$.
- [51] Notice the similarity between this phenomenon and that occurring in the ferroelectric materials where the electric-dipolar interaction drives the softening of the phonon frequency.
- [52] E. Y. Andrei, **Two-Dimensional Electron Systems on Helium and other Cryogenic Substrates** ,(Kluwer Academic Publ. 1997) , pags.245-279 and refs. therein.
- [53] E. Y. Andrei , Phys. Rev. Lett. **52** , 1449 (1984).
- [54] C. C. Grimes , G. Adams, Phys. Rev. Lett. **42**, 795 (1979).
- [55] D. S. Fisher, B. I. Halperin , P. M. Platzman , Phys. Rev. Lett. **42** , 798 (1979).
- [56] S. N. Klimin, V. M. Fomin J. Tempere, I. F. Silvera, J. T. Devreese, Sol. Stat. Comm. **126**, 409 (2003).
J. Tempere, S. N. Klimin, I. F. Silvera J. T. Devreese, Eur. Phys. J. B **32**, 329 (2003).